Mon. Not. R. Astron. Soc. **000**, 1–21 (2009) Printed 7 October 2014 (MN LATEX style file v2.2)

Black Hole Spin Evolution Affected by Magnetic Field Decay

Anna Chashkina ⋆ and Pavel Abolmasov
Sternberg Astronomical Institute, Moscow State University, Moscow, Russia 119992

arXiv:1410.1203v1 [astro-ph.HE] 5 Oct 2014

Accepted —. Received —; in original form —

ABSTRACT

Black holes are spun up by accreting matter and possibly spun-down by magnetic fields. In our work we consider the effect on black hole rotation of the two electromagnetic processes, Blandford-Znajek and Direct Magnetic Link, that differ in their magnetic field configuration. The efficiency of these processes varies with mass accretion rate and accretion regime and generally result in an equilibrium spin parameter in the range from 0.35 to $\sim$ 0.98. Magnetic field loses its energy while being accreted that may lead to an increase in equilibrium Kerr parameter for the case of advection-dominated disc. We find magnetic field decay decay can decrease electromagnetic term significantly thus increasing the Kerr parameter. We have performed Monte-Carlo simulations for a supermassive black hole population. Our simulations show broad distributions in Kerr parameter ($0.1 \lesssim a \lesssim 0.98$) with a peak at $a \sim 0.6$. To explain the high observational Kerr parameter values of $a \gtrsim 0.9$, episodes of supercritical accretion are required. This implication does not however take into account black hole mergers (that play an important role for supermassive black hole evolution).

Key words: Physical data and processes: Black hole physics – Physical data and processes: Magnetic fields

1 INTRODUCTION

Stellar mass black holes (BH) are the final stage of the evolution of the most massive stars. Supermassive black holes (SMBH) can be formed by accretion onto stellar mass BH or by mergers of stellar mass and intermediate mass BHs, but this question now is open (see Shankar (2009) and Haiman (2013) for review). Any BH is characterized by its mass M and its total angular momentum J. These parameters may evolve under the influence of different processes, primarily due to accretion of matter. There are two types of objects where the black hole mass grows significantly during their evolution: black holes in some X-ray binaries such as X-ray novae and SMBH in galactic nuclei.

Black holes are believed to be spun up by gas accretion. For the standard thin disc case the net angular momentum of the material at the innermost stable circular Keplerian orbit (having radius R_{in}) always exceeds this of the black hole itself, the latter limited by the value GM/c. Below we will use relativistic dimensionless quantities $j^\dagger = L^\dagger(R_{in})/(GM/c)$ (specific angular momentum in GM/c units) and $E^\dagger$ (dimensionless specific energy at infinity for a particle at R_{in}) following the designations used by Page & Thorne (1974). We also describe BH rotation in terms of its Kerr parameter $a = Jc/GM^2 < 1$.

Inside R_{in} accreting matter conserves its angular momentum, hence the black hole is spun up according to a simple law $da/d\ln M = \left(\frac{j^\dagger}{E^\dagger} - 2a\right) \times \mu$, where $\mu \simeq 1$ is dimensionless specific enthalpy (Beloborodov et al. 1997) and accounts for internal energy contribution to the total (relativistic) mass accretion rate. In advection-dominated regime and supercritical accretion these assumptions are violated due to non-Keplerian rotation and transonic structure of the disc, where angular momentum can be transferred by stresses inside the last stable orbit (see Abramowicz et al. (2010) and sec. 3).

Black hole spin evolution has been considered by more than forty years, since Bardeen (1970) obtained an analytical

⋆ E-mail: sagitta.minor@gmail.com

© 2009 RAS

solution for black hole spin-up by accretion. Since then, several processes were proposed that may stop this spin-up at higher or lower spin values. First of all, selective capture of accretion disc radiation in Kerr metric is able to provide a strong counteracting spin-down torque if the BH rotation parameter is close to maximal. Due to this reason, it is impossible to spin up black holes to very high a (Thorne 1974). Dimensionless spin parameter stalls at a value ~ 0.998, when the spin-up is compensated by the angular momentum of the captured photons emitted by the inner parts of the flow.

The work by Kato et al. (2010) proposes that Blandford-Znajek process (Blandford & Znajek 1977) may be responsible for black hole spin settling somewhere around $0.4-0.5$. The power of this process is determined by the Poynting flux generated by poloidal magnetic field and toroidal electric field induced by black hole rotation. Radio-bright active galactic nuclei (AGNs) and microquasars are supposed to power their jets via the Blandford-Znajek mechanism. At the end of XX century alternative mechanism known as direct magnetic link was proposed (see Uzdensky (2005) and references therein). Below we use the name DML (direct magnetic link) for any process of magnetic-field mediated angular momentum exchange between the BH and accretion disc.

Magnetic field in this case connects the black hole with the accretion disc. Depending on relation between the angular velocities of the black hole and the accretion disc, black hole can spin-up or spin-down. This mechanism differs from Blandford-Znajek process in its magnetic field geometry (see the next section and Uzdensky (2005), Krolik (1999)). If magnetic flux through the disc is not zero, flux can be accumulated inside the last stable orbit that leads to Blandford-Znajek geometry. This is confirmed by many simulations (see for example McKinney et al. (2012)). In our work we will consider black hole spin evolution taking into account both electromagnetic mechanisms: Blandford-Znajek process and DML. We will describe these processes in detail in the next section.

It should be noted that magnetic fields dissipate at the vicinity of the event horizon. Below, we use membrane paradigm (Thorne et al. 1986) to estimate "Joule losses" at the stretched horizon and the power that magnetic fields extract from black hole rotation. One actually needs accretion to supply the magnetic field. In this paper, we estimate the effect of magnetic field decay for constant mass accretion rate. Note that magnetic field can not dissipate in BZ case because magnetic flux is conserved and the field can be supported by currents in the disc.

In the following section, we discuss the basic properties of the basic electromagnetic field configurations, in section 3 we use membrane paradigm to estimate the angular momentum and energy extracted from a rotating black hole by magnetic fields for these configurations. In section 4, we discuss the influence of magnetic field decay. We present our results in section 5 and discuss them in section 6. In section 5 we also present some applications supermassive and stellar mass black holes.

2 POWER AND SPIN-DOWN RATE

In our work we use Membrane paradigm (Thorne et al. 1986) that helps describe the black hole horizon avoiding complicated general relativity calculations.

Recent numerical results such a jet simulations support the capability of this approach to reproduce the main features of black hole magnetospheres and accretion flows

(Penna et al. 2013).

In the Membrane approach framework (Thorne et al. 1986), the event horizon is considered surrounded by the so-called stretched horizon – viscous conducting sphere that has finite entropy and does not conduct heat. This sphere rotates with angular velocity $\Omega_H = \frac{a}{2}\frac{c}{R_H}$, here $R_H = \left(1+\sqrt{1-a^2}\right) GM/c^2 = r_H GM/c^2$ is horizon radius. Using this paradigm, properties of a black hole can be considered without complicated general relativistic calculations. This approach is sufficient for our needs.

There are two main electromagnetic processes that affect the rotational evolution of a black hole: Blandford-Znajek process (Blandford & Znajek 1977) and direct magnetic link (Uzdensky 2005). The main difference between these processes is in magnetic field configuration. Blandford-Znajek process works when field lines connect the black hole with a distant region such as jet [1] (Fig. 1, right). In DML case magnetic lines connect the stretched horizon with the accretion disc (Fig. 1, left).

One can describe a black hole magnetosphere as a steady and axisymmetric system of nested electric circuits consisting of a battery and a load. The battery here is the warped space region near the black hole, and the jet or accretion disc plays the role of the load.

Poloidal magnetic field:

$$\vec{B_p} = \frac{(\nabla\Psi)\times e_{\hat{\phi}}}{2\pi\varpi} \tag{1}$$

[1] We do not need the jet to be collimated for the Blandford-Znajek process to operate. Jet collimation occurs at the distances much larger than characteristic scales where black hole rotation energy is converted into electromagnetic (Tchekhovskoy et al. 2010). Collimation can be produced by some surrounding media such as thick disc or intense disk wind. Numerical simulations such as Fragile et al. (2012) also suggest that jet collimation is not directly connected to disc thickness but rather to existence of disc corona or wind providing the necessary pressure.

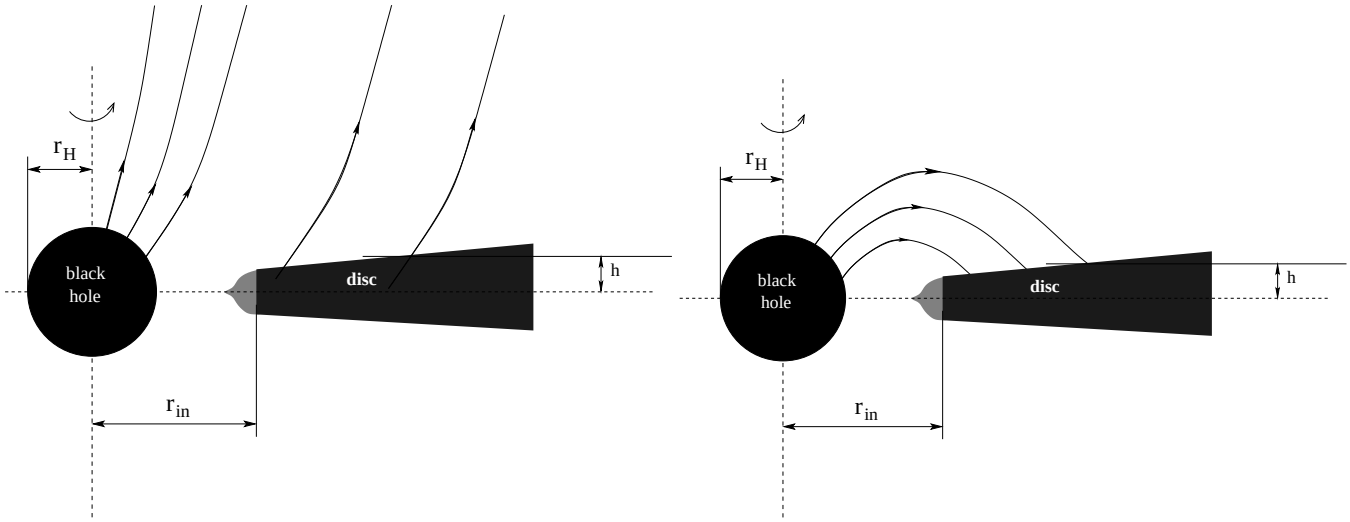

Figure 1. Magnetic field configuration for Blandford-Znajek (left) and Direct Magnetic Link (right) cases.

here Ψ is magnetic flux, ϖ is the radial cylindric coordinate. Field lines in such configuration rotate as a rigid body with Ferraro angular velocity Ω_F (Ferraro 1937). In a force-free magnetosphere magnetic field is degenerate, $\vec{E} \cdot \vec{B} = 0$, and one can write electric field as follows:

$$\vec{E} = -\frac{(\Omega_F - \omega)}{2\pi\alpha_l}\nabla\Psi \tag{2}$$

where ω is Lense-Thirring precession frequency and α_l is the lapse function taking in account dilation of time.

The electromotive force produced by the gravitational field:

$$\Delta V = \oint \alpha_l \vec{E} d\vec{l} = \frac{1}{2\pi}\Omega_H \Delta\Psi \tag{3}$$

This electromotive force is balanced by the potential difference along the horizon surface and potential difference in the load region:

$$\Delta V = \Delta V_H + \Delta V_L \tag{4}$$

The potential difference along the horizon part of the current:

$$\Delta V_H = \oint \alpha_l \vec{E} d\vec{l} = \frac{1}{2\pi}(\Omega_H - \Omega_F)\Delta\Psi \tag{5}$$

One can find a potential difference within the load using eq. (4) and eq. (5) as follows:

$$\Delta V_L = \frac{1}{2\pi}\Omega_F \Delta\Psi \tag{6}$$

Resistance of a horizon belt of latitudinal size Δl:

$$\Delta R_H = R_H \frac{\Delta l}{2\pi\varpi} = R_H \frac{\Delta\Psi}{4\pi^2\varpi^2 B_n} \tag{7}$$

here $R_H = 4\pi/c = 377$ Ohm is specific horizon surface resistivity, B_n is normal component of magnetic field at the horizon, Δl is elementary distance along the horizon between two magnetic layers. Since $I = \text{const}$ inside a given flux tube,

$$\frac{\Omega_F}{\Omega_H - \Omega_F} = \frac{\Delta V_L}{\Delta V_H} = \frac{\Delta R_L}{\Delta R_H} \tag{8}$$

Taking into account that $\Delta V_L = I\Delta R_L$ and $\Delta V_H = I\Delta R_H$, one can write:

$$I = \frac{\Delta V}{\Delta R_H + \Delta R_L} = \frac{1}{2}(\Omega_H - \Omega_F)\varpi^2 B_n \tag{9}$$

Total Joule losses for an elementary circuit are $\Delta P = I\Delta V$.

Dissipative power at the horizon:

$$\Delta P_H = \frac{(\Omega_H - \Omega_F)^2}{4\pi}\varpi^2 B_n \Delta\Psi \tag{10}$$

Power transferred by Poynting vector towards the load equals:

$$\Delta P_L = \frac{\Omega_F(\Omega_H - \Omega_F)}{4\pi}\varpi^2 B_n \Delta\Psi \tag{11}$$

The total energy losses towards the load may be found by integrating ΔP_L over the magnetosphere:

$$\frac{dE}{dt} = \int_\Psi \delta P_L = \frac{1}{8c}\Omega_F(\Omega_F - \Omega_H) r_H^4 \langle B_p^2 \rangle \tag{12}$$

Angular momentum losses may be calculated by integrating the $r\varphi$- component of the Maxwell stress tensor:

$$\frac{dJ}{dt} = \int_\Psi \frac{1}{4\pi} B_\phi B_p \cdot 2\pi\varpi^2 \delta\Psi = \frac{1}{8c}(\Omega_F - \Omega_H) r_H^4 \langle B_p^2 \rangle \tag{13}$$

Since energy and angular momentum losses differ by the factor of Ω_F, we can interpret them as extraction of rotational energy from the black hole.

Depending on the difference between Ω_F and Ω_H, energy and angular momentum may be either absorbed by the black hole or extracted from it by magnetic fields. The main difference between the two configurations, Blandford-Znajek and direct magnetic link, is in the value of Ferraro frequency. For the Blandford-Znajek case, relation between Ω_H and Ω_F is determined by the unknown resistance of the distant load. Below we assume $\Omega_F = \Omega_H/2$ in the case of Blandford-Znajek configuration, that corresponds to maximal energy extraction rate from black hole rotation.

We assume that magnetic field is in equipartition with gas+radiation as $\frac{B_p^2}{8\pi} = \frac{1}{\beta}p$, where p is total thermal pressure, and β is a dimensionless coefficient about unity.

Finally, we write the two dynamical equations (12,13) for Blandford-Znajek process as follows:

$$\frac{dE}{dt} = \frac{\pi}{\beta}\frac{\Omega_H^2 R_H^4 p}{4c} \tag{14}$$

$$\frac{dJ}{dt} = \frac{\pi}{\beta}\frac{\Omega_H R_H^4 p}{2c} \tag{15}$$

In the case of direct magnetic link the effective black hole conductivity is much smaller than the conductivity of the ionized plasma of the disc. Therefore, magnetic field may be considered frozen into the disc at some effective radius r_{eff} close to the last stable orbit radius r_{in}. The pressure inside a standard disc (in gas pressure dominated zone, (Shakura & Sunyaev 1973) is close to the maximal value at the distance of $1.3r_{in}$, hence we assume $r_{eff} = 1.3r_{in}$ in our calculations. Ferraro frequency equals Kepler frequency at the effective radius, $\Omega_F = \Omega_K(r_{eff})$.

For higher rotation parameters, Keplerian frequency at the inner face of the disc is lower than the frequency Ω_H, and black hole rotation energy is transferred to the disc. The innermost stable orbit corotates with the stretched horizon at $a = a_{cr} \simeq 0.3594$ (Uzdensky 2005), for $r_{eff} = 1.3r_{in}$, the corresponding critical value is $a_{cr} \sim 0.218$. It can be checked that for $a > a_{cr}$ magnetic field slows down or stops black hole spin-up, and sometimes is proposed to stop accretion (Agol & Krolik 2000) by creating a non-zero torque at the inner boundary of the disc.

Magnetic field lines in the case of direct magnetic link connect disc to the stretched horizon, therefore the magnetic field strength should be modified by a factor determined by geometry. Magnetic flux conservation implies:

$$R_H h_H B_p^H = 2hR_{eff} B_p^{disc}$$

Here, h_H is the width of the equatorial band at the horizon surface that is connected to the disc, h is disc half-thickness at the r_{eff}. Left- and right-hand sides correspond to the flux at the horizon and at the surface of the disc at r_{eff}. Finally, the energy and angular momentum transmitted by direct magnetic link may be expressed in a form similar to eqs. (14,15):

$$\frac{dE}{dt} = \frac{\pi}{\beta c}\Omega_K(r_{eff})(\Omega_K(r_{eff}) - \Omega_H) R_H^2 R_{eff}^2 p \left(\frac{h}{h_H}\right)^2 \tag{16}$$

$$\frac{dJ}{dt} = \frac{\pi}{\beta c}(\Omega_K(r_{eff}) - \Omega_H) R_H^2 R_{eff}^2 p \left(\frac{h}{h_H}\right)^2 \tag{17}$$

In our calculations we assume $h_H = R_H$.

The question may arise whether these two magnetic field configurations are the only ones allowed for accretion disks. The geometry of seed magnetic fields may be different but as long as we consider axisymmetric configurations such as accretion disks the possible zoo of magnetic field configurations is limited. One can expand magnetic field in multipoles. In general,

every magnetic field configuration will consist of some uniform part and higher multipoles that should be confined inside the falling matter. Note that magnetic loop curvature leads to Lorentz force that makes some configurations unstable (such as the conventional DML case shown in figure 1, right panel). Our consideration of DML does not depend on the characteristic magnetic field spatial scales in the disk as long as radial motions are much faster inside the last stable orbit.

3 ROTATIONAL EVOLUTION

In this section we estimate the electromagnetic terms in rotational evolution for different accretion regimes. It is convenient to normalize all characteristic timescales to Eddington time $t_{Edd} = c\varkappa/4\pi G \sim 0.4$Gyr that is the characteristic time for Eddington-limited accretion mass gain. In this section we use time normalized to Eddington time $\tau = t/t_{Edd}$, where $\varkappa$ is Thomson (electron scattering) opacity. A general expression for Kerr parameter evolution is:

$$\frac{da}{d\tau} = \frac{c}{G}\left(\frac{1}{M^2}\frac{dJ}{d\tau} - \frac{2aG}{Mc^3}\frac{dE}{d\tau}\right) \tag{18}$$

3.1 Accretion disk models

In this subsection we give a small introduction to different accretion models and try to describe some of their limitations.

Standard disc model by Shakura & Sunyaev (1973) now is the most widely used for intermediate accretion rates $\dot{M} \sim 0.01 - 1\dot{M}_{Edd}$. In this model, there are at least three basic assumptions. One is "alpha-prescription", i.e. the assumption that viscous stress is proportional to thermal (gas+radiation) pressure with some coefficient α constant throughout the disk, $W_{r\phi} = \alpha p$. The second assumption is that accretion disk is geometrically thin that implies that the thermal velocity and the radial velocity are much smaller than Keplerian velocity, and all the energy dissipated by viscous processes is radiated locally. The thinness of the standard disc makes it difficult to simulate numerically. We use relativistic version of the model (Novikov & Thorne 1973) in our calculations. Third, less frequently mentioned, assumption is the boundary condition at the inner edge of the disk where the viscous stress is assumed to be zero. Near the last stable orbit, some of the standard disk assumptions are violated. Firstly, near the last stable orbit the radial velocity can become comparable to Keplerian. Another thing is viscous stress tensor may deviate from zero near the last stable orbit. In a more comprehensive analysis, boundary condition is non-trivial that may be viewed as a torque applied to the inner edge of the disc. It contributes to angular momentum exchange between accretion disk and black hole that may be effectively incorporated in the DML term.

For very large and very small accretion rates one should take into account advection process that makes accretion disk geometrically thick.

For low accretion rates $\dot{M} \lesssim 0.01\dot{M}_{Edd}$ we use ADAF model by Narayan & Yi (1995) that describes a geometrically thick disk with radial energy advection, that has some non-negligible radial pressure gradient and radial velocity. Narayan& Yi's model is essentially self-similar hence all the velocities are locally proportional to the Keplerian velocity. The self-similar nature is the main disadvantage of this ADAF model since boundary conditions cannot be satisfied. The other problem is its instability to thermal perturbations (Blandford 2002). This model can explain some observational results (Mahadevan 1998), but other observations and simulations indicate the insufficiency of ADAF approach (Oda et al. 2012). The main advantage of this model is its simplicity and the existence of analytical expressions for all the quantities such as gas pressure and the thickness of the disk.

The other model applied for low accretion rates is a modification of ADAF, Advection-dominated inflow-outflow solution – ADIOS (Blandford & Begelman 1999). Apart from advection, this model also takes into account isotropic wind from the disk. Therefore, only a small fraction of the accreting matter falls onto the BH. Note however that for hydrodynamical disks, radiative inefficiency does not directly imply formation of massive outflows, as it was shown by Abramowicz et al. (2000) using analytical arguments.

The only model that consistently considers the transonic nature of the flow near the last stable orbit is the slim disk by Abramowicz et al. (1988). Slim disk may be thought of as a standard disk where the assumptions of negligibility of pressure gradient and $(\mathbf{v}\nabla)\mathbf{v}$ terms in Euler equations are relaxed. This model can be applied to any accretion disk within a wide range of accretion rates. The main reason why we do not use this model is lack of analytical solutions for the equation set defining the slim disk.

Supercritical accretion was considered with help of the model by Lipunova (1999) and its modified version by Poutanen et al. (2007) . This model is a generalization of the Shakura-Synaev's model for super-Eddington accretion rates. Unlike the slim-disk approach, it takes into account the loss of accreting material in the disk wind but includes advection that is important for large accretion rates. Numerical simulations confirm existence of outflows (see Ohsuga et al. (2005), Fukue (2011), Yang et al. (2014)). However, some recent numerical results (Sadowski et al. 2014) argue for a more complex structure of the flow where winds exist at distances larger than the classical non-relativistic spherization radius but mass accretion rate is practically

constant with radius in the inner parts of the disk. This may imply that the real mass accretion rates are several times larger in the super-critical case. This allows black holes to grow more rapidly than expected in the naïve non-relativistic approach but does not alter significantly the expected spin-up curve that we find indistinguishable from the dust-like solution (see below section 5.2.3).

Surely, there is a lot of limitations and simplifications in the models we use. But we hope that does not contribute significantly to our results. In discussion we consider some possible consequences of the over-simplifications introduced by the models used in our work.

3.2 Standard disc

Falling matter with high angular momentum forms an accretion disc around a black hole. As we have already mentioned above we used the relativistic version of Shakura-Sunyaev's model introduced by Novikov & Thorne (1973). This accretion regime apparently occurs in outbursts of X-ray novae and in the bright AGNs (Seyfert galaxies and QSOs). In this model, the accretion disc is considered geometrically thin and optically thick and is divided into three zones A, B and C depending on the terms dominating pressure and opacity. Since we study the hottest inner parts of the accretion disc, only zones A and B were considered, where the main opacity contribution is electron scattering. Gas and radiation pressure dominate in zones B and A, respectively.

$$p(r) = \begin{cases} 1.93 \cdot 10^{16} \alpha^{-1} m^{-1} r^{-3/2} \mathcal{A}^{-2} \mathcal{B}^{2} \mathcal{S} \ \mathrm{erg\,cm^{-3}} & \text{zone A} \\ 2.65 \cdot 10^{18} \alpha^{-9/10} m^{-17/10} \dot{m}^{4/5} r^{-51/20} \mathcal{A}^{-1} \mathcal{B}^{1/5} \mathcal{D}^{-2/5} \mathcal{S}^{1/2} \mathcal{F}^{4/5} \ \mathrm{erg\,cm^{-3}} & \text{zone B} \end{cases} \tag{19}$$

Here $\mathcal{A}, \mathcal{B}, \mathcal{C}, \mathcal{D}, \mathcal{F}, \mathcal{S}$ are relativistic correction factors (see Penna et al. (2012)).

The boundary between these zones is determined by equality between radiation and gas pressures and lies at $r = r_{ab}$:

$$r_{ab} = 96 \alpha^{2/21} m^{2/21} \dot{m}^{16/21} \mathcal{A}^{20/21} \mathcal{B}^{-12/7} \mathcal{D}^{-8/21} \mathcal{S}^{-10/21} \mathcal{F}^{16/21} \tag{20}$$

For a low accretion rates, effective radius is situated in zone B, and for accretion rates higher than $\sim 0.2 \dot{M}_{Edd}$ (for $M = 10^7 M\odot$) in zone A.

In our calculations we used viscosity parameter α equal to 0.1 and dimensionless coefficient β equal to 1. Variations of these parameters will be discussed in sec. 5.2. Accretion rate onto a black hole and its mass were normalized to the critical accretion rate (Eddington limit L_{Edd}/c^2) and to the solar mass, respectively:

$$\dot{m} = \frac{\dot{M}}{\dot{M}_{edd}} = \frac{\dot{M} c \kappa}{4 \pi G M}$$

$$m = \frac{M}{M\odot}$$

One can re-write the main evolutionary equations (14-17) for each of the two zones A and B in the case of standard relativistic sub-Eddington disc using eq. (18) for the pressure and Keplerian frequency as viewed from infinity $\Omega_K = \frac{c^3}{GM}(r_{eff}^{3/2} + a)^{-1}$ at effective radius $r_{eff} = 1.3 r_{in}$ as follows:

3.2.1 Zone A

$$\left(\frac{dE}{d\tau}\right)_{em} = \begin{cases} 0.017 M_\odot c^2 \times \alpha^{-1} \beta^{-1} a^2 r_H^2 m {r_{eff}}^{-3/2} \mathcal{A}^{-2} \mathcal{B}^{2} \mathcal{S} & \text{BZ} \\ 0.322 M_\odot c^2 \times \alpha^{-1} \beta^{-1} m \dot{m}^2 {r_{eff}}^{1/2} (r_{eff}^{3/2} + a)^{-1} \left((r_{eff}^{3/2} + a)^{-1} - \frac{a}{2 r_H} \right) \mathcal{A}^{2} \mathcal{B}^{-4} \mathcal{C}^{2} \mathcal{D}^{-2} \mathcal{S}^{-1} \Phi^2 & \text{DML} \end{cases} \tag{21}$$

$$\left(\frac{dJ}{d\tau}\right)_{em} = \begin{cases} 0.07 \frac{G M_\odot^2}{c} \times \alpha^{-1} \beta^{-1} a r_H^3 m^2 {r_{eff}}^{-3/2} \mathcal{A}^{-2} \mathcal{B}^{2} \mathcal{S} & \text{BZ} \\ 0.322 \frac{G M_\odot^2}{c} \times \alpha^{-1} \beta^{-1} m^2 \dot{m}^2 {r_{eff}}^{1/2} \left((r_{eff}^{3/2} + a)^{-1} - \frac{a}{2 r_H} \right) \mathcal{A}^{2} \mathcal{B}^{-4} \mathcal{C}^{2} \mathcal{D}^{-2} \mathcal{S}^{-1} \Phi^2 & \text{DML} \end{cases} \tag{22}$$

$$\left(\frac{da}{d\tau}\right)_{em} = \begin{cases} 0.07 \alpha^{-1} \beta^{-1} a r_H^3 {r_{eff}}^{-3/2} \left(1 - \frac{a^2}{2 r_H} \right) \mathcal{A}^{-2} \mathcal{B}^{2} \mathcal{S} & \text{BZ} \\ 0.322 \alpha^{-1} \beta^{-1} \dot{m}^2 {r_{eff}}^{1/2} \left((r_{eff}^{3/2} + a)^{-1} - \frac{a}{2 r_H} \right) \left(1 - 2a (r_{eff}^{3/2} + a) \right) \mathcal{A}^{2} \mathcal{B}^{-4} \mathcal{C}^{2} \mathcal{D}^{-2} \mathcal{S}^{-1} \Phi^2 & \text{DML} \end{cases} \tag{23}$$

3.2.2 Zone B

$$\left(\frac{dE}{d\tau}\right)_{em} = \begin{cases} 2.1 M_\odot c^2 \times \alpha^{-9/10}\beta^{-1} a^2 r_H^2 m^{11/10}\dot{m}^{4/5} {r_{eff}}^{-51/20}\mathcal{A}^{-1}\mathcal{B}^{1/5}\mathcal{D}^{-2/5}\mathcal{S}^{1/2}\Phi^{4/5} & \text{BZ} \\ 0.0036 M_\odot c^2 \times \alpha^{-11/10}\beta^{-1} m^{9/10}\dot{m}^{6/5} r_{eff}^{31/20}(r_{eff}^{3/2}+a)\left((r_{eff}^{3/2}+a)^{-1} - \dfrac{a}{2r_H}\right)\mathcal{A}\mathcal{B}^{-11/5}\mathcal{C}\mathcal{D}^{-8/5}\mathcal{S}^{-1/2}\Phi^{6/5} & \text{DML} \end{cases} \tag{24}$$

$$\left(\frac{dJ}{d\tau}\right)_{em} = \begin{cases} 8.39\dfrac{GM_\odot^2}{c} \times \alpha^{-9/10}\beta^{-1} a r_H^3 m^{21/10}\dot{m}^{4/5} {r_{eff}}^{-51/20}\mathcal{A}^{-1}\mathcal{B}^{1/5}\mathcal{D}^{-2/5}\mathcal{S}^{1/2}\Phi^{4/5} & \text{BZ} \\ 0.0036\dfrac{GM_\odot^2}{c} \times \alpha^{-11/10}\beta^{-1} m^{19/10}\dot{m}^{6/5} {r_{eff}}^{31/20}\left((r_{eff}^{3/2}+a)^{-1} - \dfrac{a}{2r_H}\right)\mathcal{A}\mathcal{B}^{-11/5}\mathcal{C}\mathcal{D}^{-8/5}\mathcal{S}^{-1/2}\Phi^{6/5} & \text{DML} \end{cases} \tag{25}$$

$$\left(\frac{da}{d\tau}\right)_{em} = \begin{cases} 8.39\alpha^{-9/10}\beta^{-1} a r_H^3 m^{1/10}\dot{m}^{4/5} {r_{eff}}^{-51/20}\left(1-\dfrac{a^2}{2r_H}\right)\mathcal{A}^{-1}\mathcal{B}^{1/5}\mathcal{D}^{-2/5}\mathcal{S}^{1/2}\Phi^{4/5} & \text{BZ} \\ 0.0036 \times \alpha^{-11/10}\beta^{-1} m^{-1/10}\dot{m}^{6/5} r_{eff}^{31/20}\left((r_{eff}^{3/2}+a)^{-1} - \dfrac{a}{2r_H}\right)\left(1-2a(r_{eff}^{3/2}+a)^{-1}\right)\mathcal{A}\mathcal{B}^{-11/5}\mathcal{C}\mathcal{D}^{-8/5}\mathcal{S}^{-1/2}\Phi^{6/5} & \text{DML} \end{cases} \tag{26}$$

Here BZ and DML denote Blandford-Znajek scenario and direct magnetic link, respectively.

3.3 Advective disc

For low accretion rates ($\dot{m} \lesssim 10^{-2}$), standard accretion disc is predicted to be unstable to evaporation (Meyer & Meyer-Hofmeister 1994). In this case, accretion flows are optically thin and geometrically thick and lose inefficiently the energy released by viscous heating. In combination with efficient angular momentum transfer, this leads to a non-Keplerian flow where the heat is advected towards the black hole rather than lost with radiation. This type of accretion flows is known as Advection-Dominated Accretion Flows (ADAF).

Massive black holes in non-active (quiescent) galactic nuclei (like Sgr A*) in general show radiatively inefficient accretion having very little in common with the standard thin disc accretion picture.

There are two main effects that characterize this accretion regime in the disc: radial velocities are non-Keplerian and the disc is geometrically thick. Since there is no comprehensive relativistic analytical model for ADAF flows similar to the standard disc model, we use the non-relativistic self-similar model proposed by Narayan & Yi (1995). In this model, all velocity components at some radius are proportional to the Keplerian velocity.

In particular, the radial velocity component is $v_r(R) = -\dfrac{(5+2\epsilon)}{3\alpha^2}\left(\left[1+\dfrac{18\alpha^2}{(5+2\epsilon)^2}\right]^{1/2}-1\right)v_K(R) = -c_1\alpha v_K(R)$, where $0 < c_1 < 1$. Angular rotational frequency $\Omega(R) = \left(\dfrac{2\epsilon(5+2\epsilon)}{9\alpha^2}\left(\left[1+\dfrac{18\alpha^2}{(5+2\epsilon)^2}\right]^{1/2}-1\right)\right)^{1/2}\dfrac{v_K}{R} = c_2\dfrac{v_K}{R}$. Speed of sound squared $c_s^2(R) = \dfrac{2(5+2\epsilon)}{9\alpha^2}\left(\left[1+\dfrac{18\alpha^2}{(5+2\epsilon)^2}\right]^{1/2}-1\right)v_K(R) = c_3 v_K^2(R)$.

In our simulations we use $\alpha = 0.1$ and $\epsilon = 1$, implying $c_1 = 0.43$, $c_2 = 0.53$ and $c_3 = 0.285$.

One more correction should be made connected to the high temperature of the accreted gas. One can estimate dimensionless specific enthalpy as follows:

$$\mu = 1 + \frac{U+\Pi}{\Sigma c^2} = 1 + \frac{5}{4}\frac{\Pi}{\Sigma c^2} = 1 + \frac{5}{4}\frac{p}{\rho c^2} = 1 + \frac{5}{4}\frac{c_3}{r} \tag{27}$$

Here, Σ and Π are vertically integrated mass density ρ and pressure p. Black hole spin evolution in absence of electromagnetic terms for ADAF regime is described by the following equation:

$$\frac{da}{dt} = \mu\frac{\dot{M}}{M}\left(c_2 j_K^\dagger(r_{in}) - 2aE^\dagger(r_{in})\right) \tag{28}$$

The main evolutionary equations for the case of conventional advective flow are the following:

$$\left(\frac{dE}{d\tau}\right)_{em} = \begin{cases} \dfrac{\sqrt{5}}{320} M_\odot c^2 \times \alpha^{-1}\beta^{-1} c_1^{-1} c_3^{1/2} a^2 r_H^2 r_{eff}^{-5/2} m\dot{m} & \text{BZ} \\ \dfrac{\sqrt{5}}{8} M_\odot c^2 \times \alpha^{-1}\beta^{-1} c_1^{-1} c_3^{3/2}\Omega_* m r_{eff}^{3/2}\left(\Omega_* - \dfrac{a}{2r_H}\right)\dot{m} & \text{DML} \end{cases} \tag{29}$$

$$\left(\frac{dJ}{d\tau}\right)_{em} = \begin{cases} \frac{\sqrt{5}}{80}\frac{GM_\odot^2}{c} \times \alpha^{-1}\beta^{-1}c_1^{-1}c_3^{1/2} a r_H^3 r_{eff}^{-5/2} m^2 \dot{m} & \text{BZ} \\ \frac{\sqrt{5}}{8}\frac{GM_\odot^2}{c} \times \alpha^{-1}\beta^{-1}c_1^{-1}c_3^{3/2}\left(\Omega_* - \frac{a}{2r_H}\right) {r_{eff}}^{3/2} m^2 \dot{m} & \text{DML} \end{cases} \quad (30)$$

$$\left(\frac{da}{d\tau}\right)_{em} = \begin{cases} \frac{\sqrt{5}}{80}\alpha^{-1}\beta^{-1}c_1^{-1}c_3^{1/2} a r_H^3 r_{eff}^{-5/2} \dot{m}\left(1 - \frac{a^2}{2r_H}\right) & \text{BZ} \\ \frac{\sqrt{5}}{8}\alpha^{-1}\beta^{-1}c_1^{-1}c_3^{3/2}\left(\Omega_* - \frac{a}{2r_H}\right) {r_{eff}}^{3/2}\left(1 - 2a\Omega_*\right)\dot{m} & \text{DML} \end{cases} \quad (31)$$

Here $\Omega_* = c_2\Omega_K$ is angular frequency for ADAF disc. The pressure is calculated in the following way:

$$p = 1.7 \times 10^{16}\alpha^{-1}c_1^{-1}c_3^{1/2}\dot{m}m^{-1}r_{eff}^{-5/2}\mathrm{erg\,cm^{-3}} \quad (32)$$

There are some unconstrained coefficients and it is important to understand how much Kerr parameter evolution depends on their values. Numerical coefficient ϵ depends on the ratio of specific heats γ and on the fraction of advected energy f as $\epsilon = \frac{1}{f}\frac{5/3-\gamma}{\gamma-1}$. In non-relativistic case $\gamma = 5/3$, while for relativistic flow $\gamma \to 4/3$. Fully advective disc has $f = 1$. If $f \ll 1$, a large fraction of energy is locally radiated and the disc rapidly becomes thin. Hence we always use $f = 1$ for ADAF.

Numerical coefficients c_1 and c_3 depend weakly on parameters ϵ and α. In the range $0.1 < \epsilon < 1$, and $0.01 < \alpha < 1$, they vary by about 10%. Non-Keplerianity parameter c_2 depends on ϵ and α much stronger. Near the last stable orbit, no inward-directed pressure gradient can be present hence the self-similar model probably under-estimates the value of c_2. Matter-only term is proportional to c_2, electromagnetic term is proportional to $\frac{c_2}{c_1}c_3^{3/2}$ that varies by about 18% in DML case and to $\frac{c_3^{1/2}}{c_1}$ that varies by about 21% in BZ case, hence its variations due to unknown equation of state and viscosity do not exceed ~ 0.2. If we fix c_2 equilibrium Kerr parameter varies up to 0.1% for BZ case and up to 6.5% in DML case. The largest uncertainty is connected to the unknown value of c_2. Hopefully, further, more comprehensive studies will help constrain its value.

3.4 Supercritical disc $\dot{m} >> 1$

When the accretion rate is not very low and not very high, the standard disc theory can be applied. If accretion disc luminosity reaches the Eddington limit, H/R becomes close to 1 in the inner parts of the disc and the thin disc approximation breaks down. There are at least two effects influencing the properties of supercritical accretion: outflow formation (considered in (Shakura & Sunyaev 1973)) and photon trapping (first considered in the advective Polish doughnut model (Abramowicz 2005)).

Effect of advection dominates when accretion rate is very high $\dot{m} > 10^3$. Since there is numerical support for the outflow scenario (see for example Ohsuga & Mineshige (2007)), we use an outflow-based model by Lipunova (1999). An outflow starts at the spherization radius where $H/R = 1$. Below we will adopt spherization radius in the form $r_{sp} = 5/3\dot{m}$. If effective radius is less than spherization radius, accretion rate becomes smaller and effective $\dot{m}_{eff}$ may be written as follows (see Lipunova (1999) and Poutanen et al. (2007)):

$$\dot{m}_{eff} = \begin{cases} \dot{m}\frac{r}{r_{sp}}\frac{1 + 2/3r^{-5/2}}{1 + 2/3r_{sp}^{-5/2}} & r < r_{sp} \\ \dot{m} & r > r_{sp} \end{cases} \quad (33)$$

The matter flowing from the region inside the spherization radius removes angular momentum. Radial flux of angular momentum is:

$$g(r) = \begin{cases} \frac{\dot{m}r^{3/2}}{3r_{sp}}\frac{1 - r^{-5/2}}{1 + 2/3r_{sp}^{-5/2}} & r < r_{sp} \\ \frac{\dot{m}\sqrt{r}}{3}\frac{1 - r_{sp}^{-5/2}}{1 + 2/3r_{sp}^{-5/2}} + \dot{m}(\sqrt{r} - \sqrt{r_{sp}}) & r > r_{sp} \end{cases} \quad (34)$$

Taking into account the features of supercritical regime, mass and spin evolution is described by the following equations:

$$\left(\frac{dE}{d\tau}\right)_{em} = \begin{cases} 0.02 M_\odot c^2 \times \alpha^{-1}\beta^{-1} a^2 r_H^2 {r_{eff}}^{-1} \dot{m}_{eff} r_{in}^{-1/2} m g(r_{eff})^{-1} \dfrac{1-\left(\frac{r_{eff}}{r_{in}}\right)^{-5/2}}{1+\frac{2}{3}\left(\frac{r_{eff}}{r_{in}}\right)^{-5/2}} & \text{BZ} \\ 0.21 M_\odot c^2 \alpha^{-1}\beta^{-1}\dot{m}_{eff}({r_{eff}}^{3/2}+a)^{-1}\left(({r_{eff}}^{3/2}+a)^{-1}-\dfrac{a}{2r_H}\right) g(r_{eff}) m r_{in}^{1/2} \dfrac{1-\left(\frac{r_{eff}}{r_{in}}\right)^{-5/2}}{1+\frac{2}{3}\left(\frac{r_{eff}}{r_{in}}\right)^{-5/2}} & \text{DML} \end{cases} \tag{35}$$

$$\left(\frac{dJ}{d\tau}\right)_{em} = \begin{cases} 0.08 \dfrac{GM_\odot^2}{c} \times \alpha^{-1}\beta^{-1} a r_H^3 {r_{eff}}^{-1} \dot{m}_{eff} m^2 r_{in}^{-1/2} g(r_{eff})^{-1} \dfrac{1-\left(\frac{r_{eff}}{r_{in}}\right)^{-5/2}}{1+\frac{2}{3}\left(\frac{r_{eff}}{r_{in}}\right)^{-5/2}} & \text{BZ} \\ 0.21 M_\odot c^2 \alpha^{-1}\beta^{-1}\dot{m}_{eff}\left(({r_{eff}}^{3/2}+a)^{-1}-\dfrac{a}{2r_H}\right) g(r_{eff}) m^2 r_{in}^{1/2} \dfrac{1-\left(\frac{r_{eff}}{r_{in}}\right)^{-5/2}}{1+\frac{2}{3}\left(\frac{r_{eff}}{r_{in}}\right)^{-5/2}} & \text{DML} \end{cases} \tag{36}$$

$$\left(\frac{da}{d\tau}\right)_{em} = \begin{cases} 0.08 \alpha^{-1}\beta^{-1} a r_H^3 {r_{eff}}^{-1} \dot{m}_{eff} r_{in}^{-1/2}\left(1-\dfrac{a^2}{2r_H}\right) g(r_{eff})^{-1} \dfrac{1-\left(\frac{r_{eff}}{r_{in}}\right)^{-5/2}}{1+\frac{2}{3}\left(\frac{r_{eff}}{r_{in}}\right)^{-5/2}} & \text{BZ} \\ 0.21 \alpha^{-1}\beta^{-1}\dot{m}_{eff} r_{in}^{1/2}\left((r_{eff}^{3/2}+a)^{-1}-\dfrac{a}{2r_H}\right)\left(1-2a(r_{eff}^{3/2}+a)^{-1}\right) g(r_{eff}) \dfrac{1-\left(\frac{r_{eff}}{r_{in}}\right)^{-5/2}}{1+\frac{2}{3}\left(\frac{r_{eff}}{r_{in}}\right)^{-5/2}} & \text{DML} \end{cases} \tag{37}$$

4 MAGNETIC FIELD DECAY

4.1 Hall decay

In an accretion disc magnetic field decay is in equilibrium with magnetic field amplification by the instabilities such as MRI (Balbus & Hawley 1991) and dynamo processes (Chandrasekhar 1961). This equilibrium state is shifted inside the last stable orbit where the plasma becomes magnetically dominated (gas and radiative pressure are reduced but magnetic field stress remaines practically unchanged). In these conditions magnetic field decay is primarily due to Hall cascade (Goldreich & Reisenegger 1992). This effect does not change the total magnetic energy, but it can transfer the energy to smaller spatial scales where Ohmic decay runs faster. We assume that magnetic field lines, connecting a black hole with the disc have a curvature radius L of the order GM/c^2. Following Goldreich & Reisenegger (1992) we can write magnetic field evolution equation for magnetic field affected by Hall effect:

$$\frac{\partial \mathbf{B}}{\partial t} = \frac{-c}{4\pi n e}\nabla \times [(\nabla \times \mathbf{B}) \times \mathbf{B}] + \frac{c^2}{4\pi\sigma}\nabla^2 \mathbf{B} \tag{38}$$

The first term in this equation describes Hall cascade.

For the largest loops, one may estimate $\partial \mathbf{B}/\partial t \sim B/\tau$, $\nabla \sim 1/L$ and obtain Hall timescale as following:

$$\tau_{Hall} = \frac{4\pi n e L^2}{cB} \tag{39}$$

Here n is electron concentration and L is characteristic curvature scale. For geometrically thick flow electron concentration may be estimated as $n \simeq \dfrac{\dot{m}}{\sigma_T}\left(\dfrac{c^2}{GM}\right)$.

Characteristic Hall timescale is:

$$\tau_{Hall} = \frac{4\pi \dot{m} c e R_H^2}{\sigma_T GMB} = \frac{4\pi e}{\sigma_T B}\dot{m} r_H^2 \times \tau_{dyn} \tag{40}$$

Hall decay becomes important when $\tau_{Hall} \lesssim t_{dyn}$, when mass accretion rate is very small. Using expressions for an advective disc (section 3.3), one arrives to the following estimate:

$$\tau_{Hall} \sim 10^7 \sqrt{\dot{m}m} \times \tau_{dyn}$$

Hall drift is thus unimportant for astrophysical black holes.

The second term in eq. (38) describes Ohmic decay and its timescale $\tau_{Ohm} \propto \sigma$, but conductivity of ionized relativistic plasma is very large, hence Ohmic timescale approaches infinity.

4.2 Joule losses

In Blandford-Znajek case magnetic field lines connect the black hole horizon with a distant load. Magnetic flux is conserved, hence large-scale magnetic field having non-zero flux through the equatorial plain can not dissipate and accumulates up to equipartition. These magnetic fields may be supported by electric currents in the accretion disc where resistance and dissipation are negligibly low. When we consider classical Blandford-Znajek magnetic field configurations, there is always a non-zero magnetic flux through the equatorial plane. As long as magnetic field lines are not allowed to move outwards (that is true as long as the field is frozen-in and accretion disc is present), the magnetic flux through the region inside the last stable orbit is also conserved, and one can set a lower limit for the magnetic field strength. Hence in the BZ case, magnetic flux conservation prohibits magnetic field dissipation below certain level. In the direct magnetic link case there are always tangential magnetic fields near the black hole horizon and the currents should at least partially flow close to the horizon where effective resistance appears due to general relativity effects. Hence we will consider magnetic field decay effect only for the DML case.

Classical DML scenario involving magnetic loops extending above the disc is excluded by numerical simulations (such as Penna et al. (2010)). Instead, most of the magnetic field energy is stored in frozen-in loops that are advected with the falling matter. If magnetic fields are frozen into the free-falling matter inside the ISCO, the direction of the field should alter at least once at any radius, even close to the horizon. Magnetic field configuration is that of a driven current sheet, where dissipation is concentrated towards the middle plane and may be interpreted as magnetic field reconnection. Magnetic field dissipation leads to a magnetic torque value efficiently altered by some factor of $\chi < 1$.

To estimate the magnetic field decay rate in membrane paradigm, one may consider toroidal currents responsible for radial magnetic field direction change. The amplitude of such a current is, approximately:

$$j_\varphi = \frac{c}{4\pi}[\nabla B] \simeq \frac{c}{4\pi}\frac{B^r}{D},$$

where D is the vertical scale of the falling magnetized flow. The radial extent of the flow is about $R_{in} - R_H$. Effective surface current is thus:

$$g_\varphi \simeq \frac{c}{4\pi}\frac{R_{in}-R_H}{D}B^r$$

Magnetic field B^r here is estimated at the stretched horizon and differs from the "initial" magnetic field near the ISCO (that is close to equipartition) by the factor of disc cross-section ratio $\frac{H_{in}R_{in}}{DR}$ Magnetic field energy dissipated near the horizon may be estimated as the following integral upon the BH horizon:

$$-\dot{E}_H \simeq \frac{4\pi}{c}\int g_\varphi^2 dS$$

$$-\dot{E}_H \simeq 4\pi RH \times \left(\frac{c}{4\pi}\frac{R_{in}-R_H}{D}B^r\right)^2 \times \frac{4\pi}{c} = -8\pi\left(\frac{H_{in}}{D}\right)^2 \frac{r_{in}^2(r_{in}-r_H)^2}{r_H^2} \times \left(\frac{GM}{c^2}\right)^2 p_M c$$

This is the estimated loss of the magnetic field energy near the horizon. Note that it does not involve any processes connected to black hole rotation. Magnetic field energy input from the disc:

$$\dot{E}_D \simeq p_M \times u^r \times 4\pi H_{in}R_{in} \simeq p_M \times c\alpha\frac{H_{in}}{R_{in}} \times 4\pi H_{in}R_{in} = 4\pi\alpha\left(\frac{H_{in}}{R_{in}}\right)^3 \frac{r_{in}}{r_{in}^{3/2}+a} \times \left(\frac{GM}{c^2}\right)^2 p_M c$$

Practically always $-\dot{E}_H \gg \dot{E}_D$, and the two rates become comparable only if viscosity is high and the flow is geometrically thick. Equilibrium between field decay and replenishment requires $H_{in}/R_{in} \gtrsim 1$.

Presence of a decay mechanism may mean that the magnetic field responsible for radial transfer is generally smaller than one may expect. Inner flow thickness D close to the horizon may be estimated as $D \simeq H_{in}$

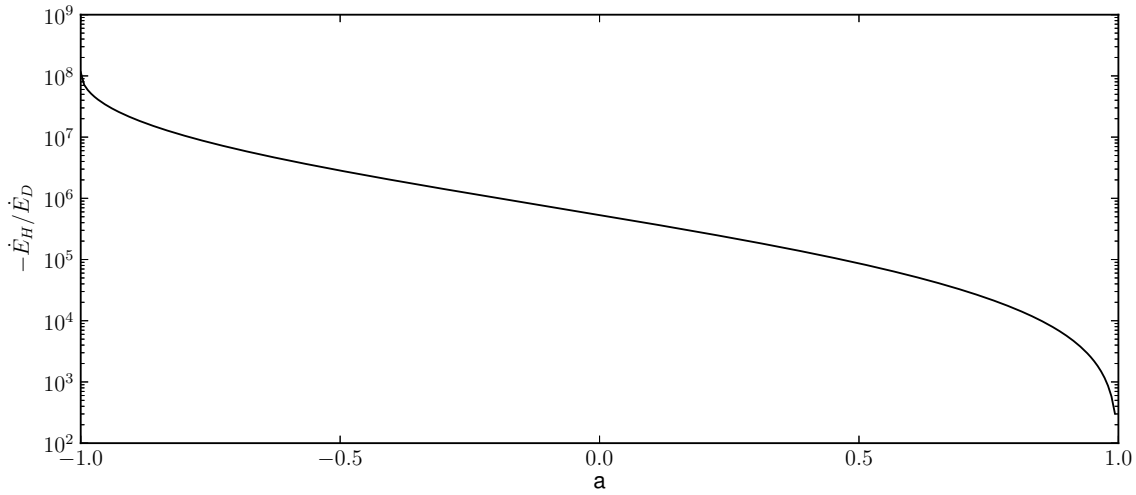

Figure 2. Ratio of magnetic field decay $\dot{E}_H$ and replenishment $\dot{E}_D$ rates as a function of Kerr parameter. Viscosity parameter $\alpha = 0.1$, disc initial thickness $H_{in} = 0.3R_{in}$.

if the flow geometry is not altered strongly by magnetic field decay itself.

$$\chi \simeq \exp\left(-t_{replenishment}/t_{decay}\right) \simeq \exp\left(\dot{E}_H/\dot{E}_D\right)$$

Substituting all the quantities:

$$\chi \simeq \exp\left(-\frac{2(r_{in}-r_H)^2 r_H}{\alpha h_{in} d^3}\right)$$

where $H_{in} = h_{in}GM/c^2$ and $D = dGM/c^2$.

Figure 2 shows the estimated decay factor as a function of Kerr parameter.

Summarizing, magnetic field decay is an important effect whenever there is tangential magnetic field component anywhere on the stretched horizon. Since magnetic field decay rate is generally several orders of magnitude larger than the rate of magnetic field replenishment from the disc (primarily because of $v_r \ll 1$), we conclude that DML momentum transfer is strongly damped.

5 RESULTS

5.1 Equilibrium Kerr parameter

Spin evolution equation may be written as:

$$\frac{da}{d\tau} = \mu\dot{m}\left[j^\dagger - 2aE^\dagger\right] + \frac{c}{G}\left[\frac{1}{M^2}\left(\frac{dJ}{d\tau}\right)_{em} - \frac{2aG}{Mc}\left(\frac{dM}{d\tau}\right)_{em}\right] \times \chi \tag{41}$$

First term here describes the Kerr parameter evolution connected to the angular momentum advected by the falling matter. It is proportional to mass accretion rate and usually positive. The second term corresponds to the contribution of electromagnetic processes described in sec. 2. This term is always negative in Blandford-Znajek regime and changes sign in the DML case when corotation radius equals the effective disc radius.

Additional multiplier χ takes into account magnetic field decay (see section 4).

As long as the first term is higher than the second by its absolute value, black hole is spun up toward $a \sim 1$ for a standard disc and up towards $a \sim 0.6$ for a sub-Keplerian ADAF disc. Here we used $j^\dagger = c_2 j_K(r_{in})$, where c_2 is a parameter taking into account deviation from Keplerian law (see section 3.3) and $j_K(r_{in})$ is net Keplerian angular momentum at the inner radius. If the second term is balanced by the first, black hole spin-up stops at the equilibrium Kerr parameter value $a_{eq} < 0.998$.

Equilibrium spin parameter dependence on accretion rate is shown in Figure 3. Solid lines correspond to the DML case and BZ is plotted by a dashed line. Red (grey) lines are hereafter used for stellar-mass black holes ($M = 10\mathrm{M}_\odot$) and black lines for SMBH ($M = 10^7\mathrm{M}_\odot$). In this figure equilibrium Kerr parameter for DML processes with magnetic field decay is plotted by dotted line (see sections 4 and 5.2.1). In ADAF regime both electromagnetic and accretion terms are proportional

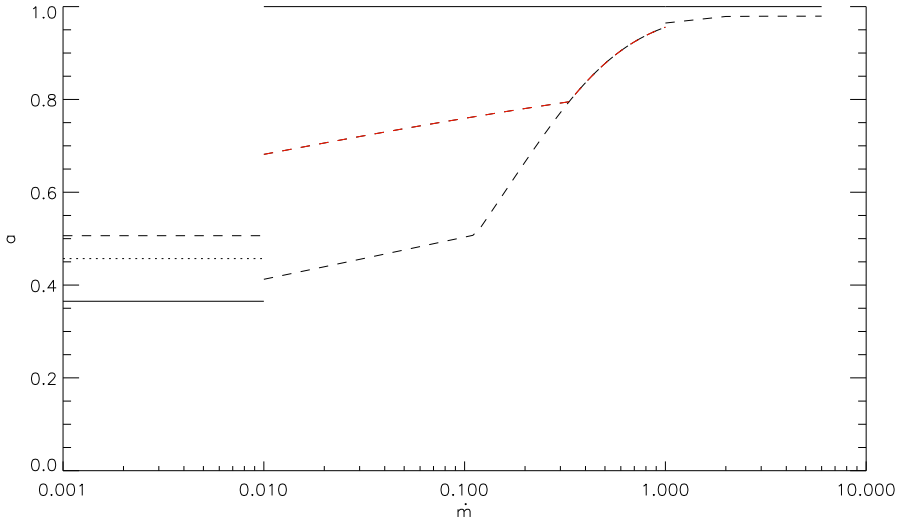

Figure 3. Equilibrium Kerr parameters for different accretion rates are plotted for BZ processes by dashed lines and for DML processes without and with magnetic field decay by solid and dotted lines respectively. Black lines correspond to SMBH ($M_0 = 10^7 M\odot$) while red (grey) lines to the stellar mass black hole ($M_0 = 10 M\odot$) case.

to accretion rate $\dot{m}$ hence the equilibrium Kerr parameter does not depend on $\dot{m}$. Also it does not depend on the BH mass that is why the solutions for supermassive and stellar-mass BHs are identical.

For the standard disc case, the breakpoint marks transition from B to A zones. For the effective radius in zone B, spin evolution strongly depends on BH mass, and the influence of the BZ process for SMBH is more significant than for LMBH. The boundary between A and B zones depends on mass and accretion rate. For LMBH this transition takes place for accretion rates greater than for SMBH. In zone A, the dependence on mass is insignificant and spin evolution proceeds in the similar way for the two types of BH. But electromagnetic term depends on $\dot{m}$ somewhat weaker than accretion term, therefore the influence of BZ processes decreases with increasing $\dot{m}$. DML in inefficient in the Standard disc case for both SMBH and LMBH.

Equation (41) has no more than one attractor in the range $-1 < a < 1$. For some parameter sets (DML+standard disc), there is no stable solution of the $da/dt = 0$ equation and the BH is spun up until $a \simeq 0.998$ where other effects not considered in this work (such as radiation capture, see Thorne (1974)) come into play. In other cases, the black hole is always spun up for $a < a_{eq}$ and spun-down for $a > a_{eq}$.

5.2 Rotational evolution of a typical SMBH

For a more detailed analysis of black hole rotational evolution we made simulations for different accretion regimes for a supermassive Kerr black hole with the following parameters: initial mass $M_0 = 10^7 M_\odot$, initial Kerr parameters $a_0 = 0$ and $a_0 = 0.7$. For arbitrary dimensionless accretion rate $\dot{m}$, both mass and spin change at characteristic timescales $\sim t_{Edd}/\dot{m}$.

For a constant non-zero accretion rate, mass grows monotonically and may be used as an independent variable.

We consider ADAF regime with accretion rate $\dot{m} = 10^{-3}$, standard disc with $\dot{m} = 0.4$ and supercritical regime with $\dot{m} = 10$. We set magnetization parameter $\beta = 1$ and $\alpha = 0.1$. Note that if viscosity is created by chaotic magnetic field stresses $\alpha \sim \dfrac{B_\phi B_r}{4\pi p} \sim \dfrac{2}{\beta}$ hence $\alpha\beta$ =const. Since the two parameters enter the equations in combination $\alpha\beta$ (save the standard disc zone B where this statement is still approximately fulfilled; see section 3), the result depends weakly on the exact value of β.

5.2.1 Rotational evolution in ADAF regime

In section 3 it was noted that spin evolution under the matter accretion contribution for ADAF regime differs from the Bardeen solution due to non-Keplerian velocity law. In Fig. 4, spin evolution for the matter-only solution is plotted with crosses, and one can see that there is an equilibrium Kerr parameter value less than unity. Spin evolution affected by the Blandford-Znajek process is plotted by a dotted line for $a_0 = 0$ and by a solid line for $a_0 = 0.7$. The dashed and dot-dashed lines show the DML case for $a_0 = 0$ and $a_0 = 0.7$, respectively . Maximal difference between BZ and sub-Keplerian matter-only solution is about 0.0067. We adopted $\epsilon' = 0.5$ that implies parameter values of $c_1 \simeq 0.43$, $c_2 \simeq 0.53$ and $c_3 \simeq 0.285$.

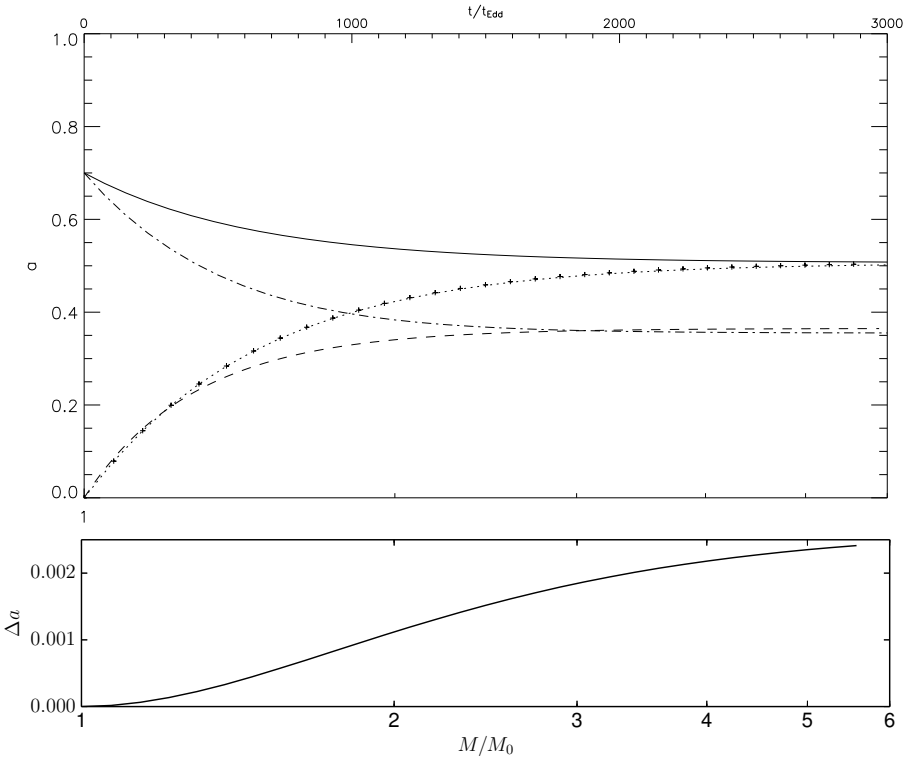

Figure 4. Spin evolution of a black hole with initial mass $M_0 = 10^7 M_\odot$, initial Kerr parameters $a_0 = 0$ and $a_0 = 0.7$, accretion rate $\dot{M} = 10^{-3}\dot{M}_{Edd}$ (ADAF regime). Unmagnetized case evolution is plotted by crosses, evolution affected by DML processes is plotted by dashed ($a_0 = 0$) and dot-dashed ($a_0 = 0.7$) lines. Evolution affected by BZ process by a dotted line for $a_0 = 0$ and by a solid line for $a_0 = 0.7$. The bottom panel shows difference in Kerr parameter between the unmagnetized (Bardeen) and Blandford-Znajek cases for $a_0 = 0$.

Electromagnetic term for DML is higher than for BZ due to the difference in numerical coefficients and in the different dependence on the effective radius. Electromagnetic terms in these two cases differ by three orders of magnitude, the DML process being more efficient. Black hole mass growth is very slow and the Kerr parameter can not increase significantly during the cosmological time if $\dot{m} \lesssim 10^{-2}$.

Note that the character of black hole rotation evolution at the timescales longer than the evolutionary time scale $t_{Edd}/\dot{m}$ is insensitive to the initial Kerr parameter.

As it was shown above (in sec.4) magnetic field decay is efficient only in the DML case. This process affects only the behaviour of the electromagnetic term in the evolutionary equation. Influence of magnetic field decay is shown in Fig. 5. Here evolution for matter contribution is plotted by a crosses, evolution affected by DML processes without and with magnetic field decay is plotted by a dotted and a solid lines, respectively. One can see that equilibrium Kerr parameter increases from 0.36 to 0.45 due to the magnetic field decay.

5.2.2 Rotational evolution in standard disc regime

The results for the standard accretion disc are presented in Fig. 6. Here again spin evolution in the Bardeen's case is shown by crosses, spin evolution affected by the Blandford-Znajek processes is plotted by dotted ($a_0 = 0$) and solid ($a_0 = 0.7$) lines and in DML case by dashed (a_0) and by dot-dashed ($a_0 = 0.7$) lines. In this case direct magnetic link is much less efficient than Blandford-Znajek processes.

Depending on magnetic field geometry, spin evolution may result either in fast rotation with $a \simeq 1$ or in an intermediate $a \simeq a_{eq}$ where matter spin-up is balanced by magnetic field spin-down. As in ADAF case, equilibrium Kerr parameter does not depend on the initial Kerr parameter value.

5.2.3 Rotational evolution in supercritical regime

In Fig. 7 we present our results for the case of supercritical regime. Here spin evolution of a black hole for matter contribution is plotted by a grey solid line, evolution affected by DML processes is plotted by dotted ($a_0 = 0$) and solid ($a_0 = 0.7$) lines.

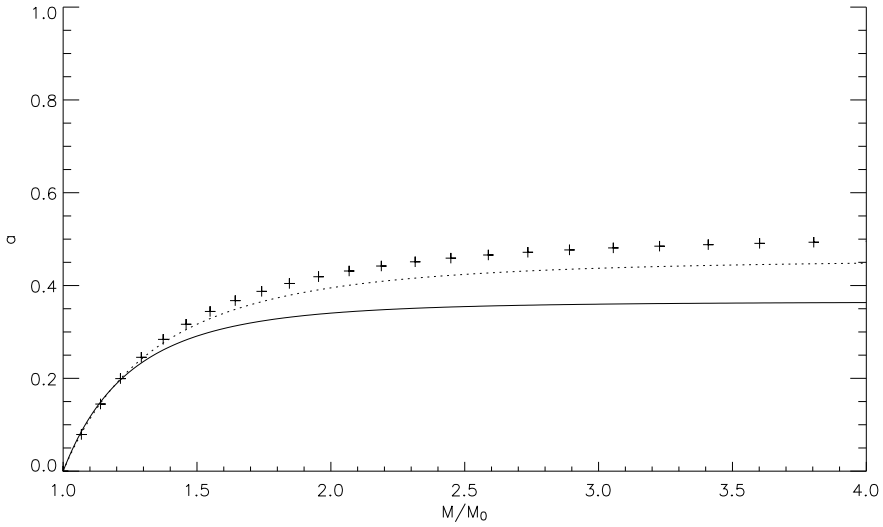

Figure 5. Spin evolution of a black hole with initial mass $M_0 = 10^7 M_\odot$, initial Kerr parameter $a_0 = 0$ accretion rate $\dot{M} = 10^{-3}\dot{M}_{Edd}$. Evolution for accretion matter contribution is plotted by crosses, evolution affected by DML processes with and without magnetic field decay are plotted by dotted line and a solid line respectively.

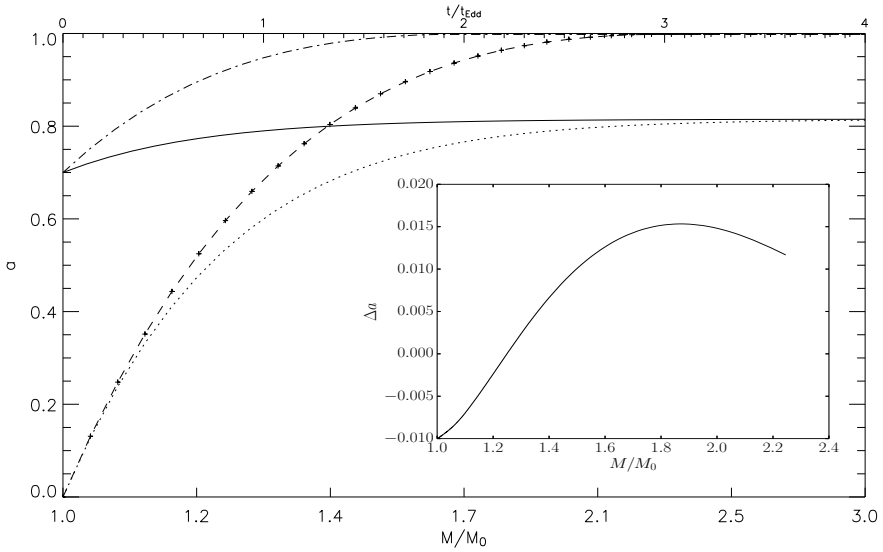

Figure 6. Spin evolution of a black hole with initial mass $M_0 = 10^7 M_\odot$, initial Kerr parameters $a_0 = 0$ and $a_0 = 0.7$, accretion rate $\dot{M} = 0.4\dot{M}_{Edd}$ (Standard disc regime). Evolution for accretion matter contribution is plotted by crosses, evolution affected by DML processes is plotted by dashed ($a_0 = 0$) and dot-dashed ($a_0 = 0.7$) lines. Evolution affected by BZ process by a dotted line for $a_0 = 0$ and by a solid line for $a_0 = 0.7$. The inset shows difference in Kerr parameter between the unmagnetized (Bardeen) and DML cases for $a_0 = 0$.

Evolution affected by BZ process by a dashed line for $a_0 = 0$ and by a dot-dashed line for $a_0 = 0.7$. The corrections to all Kerr parameters introduced by different electromagnetic processes are plotted in the inset by the same linestyles.

As it was shown above (in sec. 4) magnetic field decay is efficient only in the DML case. This process affects only the behaviour of the electromagnetic term in the evolutionary equation (41).

Note that the character of black hole rotational evolution at the timescales longer than the evolutionary time scale $t_{Edd}/\dot{m}$ is insensitive to initial Kerr parameter.

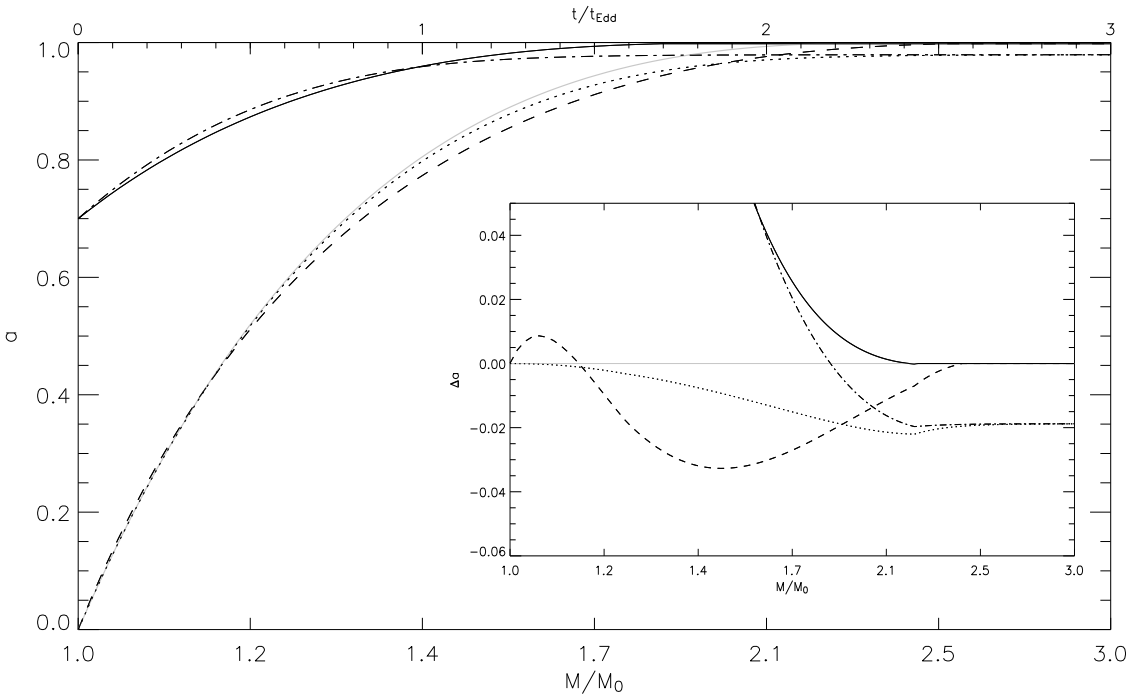

Figure 7. Spin evolution of a black hole with initial mass $M_0 = 10^7 M_\odot$, initial Kerr parameters $a_0 = 0$ and $a_0 = 0.7$, accretion rate $\dot{M} = 3\dot{M}_{Edd}$ (Supercritical regime). Evolution for accretion matter contribution is plotted by grey solid line, evolution affected by DML processes is plotted by dotted ($a_0 = 0$) and solid ($a_0 = 0.7$) lines. Evolution affected by BZ process is shown by a dashed line for $a_0 = 0$ and by a dot-dashed line for $a_0 = 0.7$.

5.3 Black holes in X-ray binaries. Comparison with observational data

X-ray binaries are usually divided into low-mass X-ray binaries (LMXB) with a donor star of several solar masses or smaller and high-mass X-ray binaries (HMXB) with the donor masses of tens of solar masses. In this section we consider spin evolution of such systems including X-ray novae and microquasars. Predictions of simple constant mass accretion rate models are compared to the observational data on several black hole X-ray binaries. We assume that initial Kerr parameters of these objects are $a_0 = 0$ since there are reasons to expect BHs to be born slowly rotating (Moreno Méndez 2011). According to the work by Podsiadlowski et al. (2003), accretion rates in these systems $\dot{m} \gtrsim 1$ hence we used a constant accretion rate model with $\dot{m} = 1$ in our calculations. We plot evolutionary tracks for black holes with masses 5, 7 and 10 $M_\odot$ in Figure 8. Solid and dashed lines represent the black hole evolution affected by Blandford-Znajek and DML processes, respectively. Here, DML is indistinguishable from Bardeen solution.

There are at least two methods used for black hole spin estimates: fitting the thermal X-ray continuum and modelling the FeKα line profile. Due to some effects such as comptonization the line profile can broaden and Kerr parameter value will be overestimated. Continuum fitting, on the other hand, allows to reproduce the jet luminosity proportionality to a^2 (Narayan et al. 2013). Therefore we used fitting results (McClintock et al. 2010) for six objects analyzed with a continuum-fitting technique. These objects are shown in Fig. 8.

This figure can be used to constrain the possible initial masses for each object and mass gains during mass exchange, these estimates given in Table 1. Electromagnetic processes do not change initial black hole mass estimates significantly, but observational spin values may be used to constrain the contribution of electromagnetic processes and possibly the mass accretion rates.

Results of our simulations are in accordance with the sources listed in a Table 1 except for the object GRS 1915+105. Mass gain of the black hole in this system is about 5 solar masses, but donor mass is much smaller. The black hole has a large Kerr parameter and mass, that suggests that this system could undergo component exchange with another system. Our estimates do not take into account the possibility of such exchange that can still be important for binary evolution. The other peculiar thing about this system is the extremely high value of $a \gtrsim 0.98$ that either requires super-critical accretion or excludes the contribution of Blandford-Znajek processes during the black hole spin-up. Since this system is currently an active microquasar, the supercritical stage scenario seems more probable.

While for microquasars, estimated spin values are usually $\gtrsim 0.5$, X-ray novae such as A 0620-00 and GRS 1124-68 are supposed to have small $a \lesssim 0.3$ (Suleimanov et al. 2008). The only exception is GRO J1655-40 that is classified both as

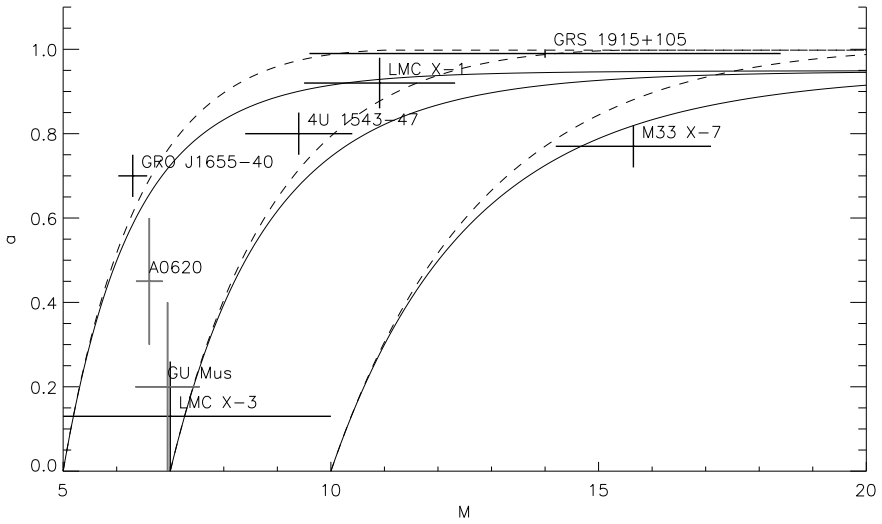

Figure 8. Spin evolution for stellar mass black holes with initial masses $M_0 = 5M_\odot$, $M_0 = 7M_\odot$ and $M_0 = 10M_\odot$. Observation data are plotted with error bars (see Podsiadlowski et al. (2003)).

Table 1. The main parameters of X-ray binary systems. Donor masses M_d, black hole masses M_{BH}, Kerr parameter a, estimated black hole initial masses M_0^* and mass gains of black holes ΔM_{BH}^*. Black holes and donor parameters were taken from: [0] - McClintock et al. (2010), [1]- Steeghs et al. (2013), [2] - Harlaftis & Greiner (2004), [3] - Shahbaz (2003), [4] - Ziółkowski (2011), [5] - Orosz et al. (2009), [6] - Hutchings et al. (2003), [7] - Orosz et al. (1998), [8] - Valsecchi et al. (2010), [11] - Casares et al. (1997), [12] -Suleimanov et al. (2008)

object names	$M_d/M_\odot$	$M_{BH}/M_\odot$	a	$M_0^*/M_\odot$	$\Delta M_{BH}^*/M_\odot$
LMC X-3	$> 13^{[6]}$	$5-11^{[0]}$	$< 0.26^{[0]}$	$4.0-9.5$	$0.3-0.5$
GRO J1655-40	$2.36-2.94^{[3]}$	$6.30\pm0.27^{[0]}$	$0.65-0.75^{[0]}$	$4.5-5.0$	~ 1.5
4U 1543-47	$2.3-2.6^{[7]}$	$9.4\pm1.0^{[0]}$	$0.75-0.85^{[0]}$	$7.0-\sim 8.0$	~ 1.3
LMC X-1	$35-40^{[4]}$, $31.79\pm3.48^{[5]}$	$10.91\pm1.41^{[0]}$	$0.92\pm0.06^{[0]}$	$6.0-7.5$	~ 3.5
GRS 1915+105	$0.47\pm0.27^{[1]}$, $0.81\pm0.53^{[2]}$	$14\pm4.4^{[0]}$	$0.98-1^{[0]}$	$5.0-9.0$	$5-10$
M33 X-7	$\sim 54^{[8]}$	15.65 ± 1.45	$0.77\pm0.05^{[0]}$	$10-12^{[0]}$	~ 4
GU Mus	$0.86\pm0.075^{[9]}$	$6.95\pm0.6^{[9]}$	$\leqslant 0.4^{[12]}$	$\sim 6-7$	$0.3-0.5$
A0620	$0.40\pm0.05^{[11]}$	$6.61\pm0.25^{[10]}$	$0.3-0.6^{[12]}$	$5.4-5.8$	~ 1

an X-ray nova and a microquasar. Donor masses in such systems are $\lesssim 1\mathrm{M}_\odot$ and the black hole mass gains are probably insufficient for significant spin-up during the evolutionary time.

Massive black hole binaries like M33 X-7 and the two objects from LMC have a broad range of spin values that conforms with the expectation that these objects should follow a nearly Bardeen spin-up track and thus can acquire $a \simeq 1$ if given sufficient time.

Our results are in a good agreement with the recent results by Fragos & McClintock (2014) who use models of stellar evolution to explain the observed correlation between black hole masses and rotation parameters in low-mass X-ray binary systems.

5.4 Monte-Carlo simulations of a SMBH population

All the evolutionary scenarios described in the previous sections are simplified models. In real life black hole evolution is more complicated. We have made population synthesis of black holes rotational evolution assuming that Blandford-Znajek and DML processes may affect black hole spin evolution simultaneously. We use the Monte-Carlo technique for population synthesis of rotational evolution of a reasonably realistic supermassive black hole population. We assume the initial masses distributed according to the log-uniform law ($dN/d\ln M = const$) between $10^6 M_\odot$ and $5\times10^8 M_\odot$. All the objects are born

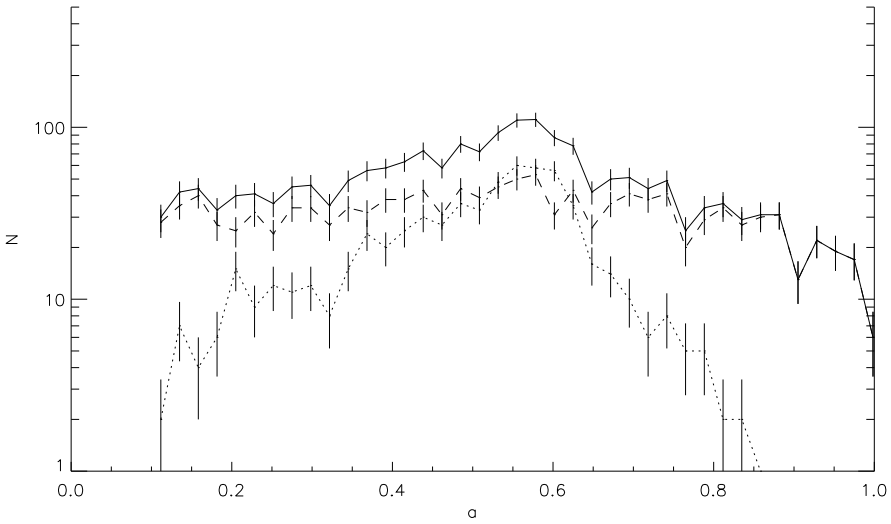

Figure 9. Kerr parameter distribution for evolved supermassive black hole population. Distribution for all population is plotted by solid line, black hole in active nuclei are plotted by dashed line and in nonactive nuclei are plotted by dotted line.

at $z = 15$. Dimensional accretion rate was chosen for each black hole and for each time bin according to a log-normal law with the dispersion of $D(\lg \dot{M}) = 0.65$ and the mode (probability maximum) at $1.3 \times 10^{-3} \mathrm{M}_{\odot}\,\mathrm{yr}^{-1}$.

For these parameter values, a conventional black hole with $M \sim 10^7 M_{\odot}$ spends $\sim 5 - 10\%$ of all time in active state that conforms to the existing duty cycle estimates (Shankar et al. 2013). Initial Kerr parameters are distributed uniformly between 0 and 1.

Here we consider the black hole active if the dimensionless accretion rate exceeds 0.01. This value is also assumed the transition mass accretion rate between standard and advective disc regimes. Supercritical disc model is applied when $\dot{m} > 1/\eta(a)$, where $\eta = 1 - E^{\dagger}$ is radiative efficiency.

We assume that Blandford-Znajek process operates in the circumpolar regions and DML operates near the equatorial plane of the black hole horizon. Simulations (McKinney et al. 2012; Barkov & Khangulyan 2012) show that magnetic lines connecting a black hole with infinity occupy much larger surface area of the black hole horizon (Blandford-Znajek process works here). Therefore we assume that the DML works in a narrow equatorial region that occupies only 10% of the black hole horizon and Blandford-Znajek process works on the remaining 90% of the surface. Existence of such a region corotating with the inner part of the disc is also confirmed by simulations (Penna et al. 2013).

Distribution of all the objects in Kerr parameter at $z = 0$ is shown in Fig. 9 with a solid line. Kerr parameter distribution for AGNs is plotted by a dashed line and quiescent nuclei are shown by a dotted line. In this figure one can see a wide distribution with a peak at intermediate Kerr parameters $a \sim 0.6 - 0.7$ that corresponds to accretion through a standard disc. Supercritical accretion regime creates the high Kerr parameter wing of the distribution. The trail to the left consists of unevolved black holes with sub-equilibrium rotation parameters of $a \sim 0.1 - 0.5$ and is produced by ADAF regime in quiescent BH like Sgr A*.

We have also performed simulations in other assumptions, but the results presented above seem the most realistic. In particular, we simulated black hole population evolution affected by the BZ process only. In this case we have only one narrow peak at $a \sim 0.5$ in contradiction with observational data (Reynolds 2013) . Another model was evolution driven solely by the DML process. This case is more interesting: there is a lot of objects with small and intermediate Kerr parameters, but there are no objects with Kerr parameters $\gtrsim 0.7$ that disagrees with the observational data.

In the recent work of Moreno Méndez (2011) the author shows that in X-ray binaries initial black hole Kerr parameters should be very small $a \sim 0$ and to explain the observed large Kerr parameters, black holes must have suffered long periods of supercritical accretion. Distribution of all objects with initial Kerr parameter uniformly distributed ($a_0 < 1$) is shown in Fig. 10. Simulations with $a_0 = 0$ and a large fraction ($\sim 10\%$) of supercritical regime are plotted by a dashed line. In the same figure distribution with uniformly distributed initial Kerr parameter described above is shown by a solid line. Distribution with $a_0 = 0$ and with a reasonable fraction of supercritical regime ($\sim 5\%$) is plotted by a dotted line. This figure shows the following features for the model with $a_0 \sim 0$: black hole evolution in sense of $a(M)$ is determined by standard disc accretion, but its timescales are longer and closer to the timescales of inefficient ADAF accretion. Hence, a lot of objects in the simulated population are unevolved. This model shows deficit in black holes with $a \gtrsim 0.6$ and this is in contradiction with observations (see McClintock et al. (2011) for review). The contribution of supercritical accretion is too small to significantly

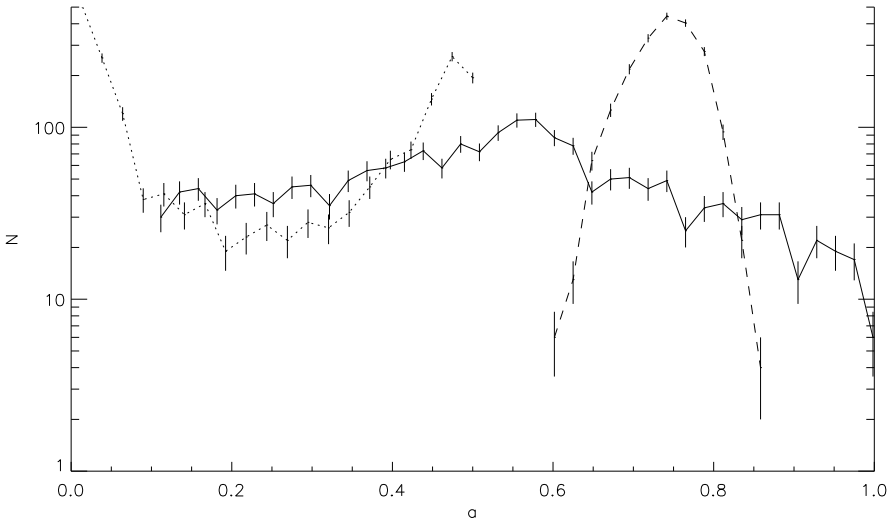

Figure 10. Distribution in Kerr parameter. Distribution with initial Kerr parameter $a_0 = 0$ is plotted with a dotted line. Distribution with uniform initial Kerr parameter $0 < a < 1$ is plotted with a solid line and with a dashed line with a large fraction ($\sim 10\%$) of supercritical regime, $a_0 = 0$.

spin up a black hole, since this regime is difficult to sustain for black holes with $m_0 > 5 \times 10^7$ and the fraction of supercritical accretors with $m_0 \sim 10^7$ is less than several percent. Subsequently all the objects accumulate mass and dimensionless accetion rate decreases. Supercritical accretion shifts the mode of the distribution towards higher Kerr parameters. The model with increased mass accretion rate (shown by a dashed line in Fig. 10) shows a lot of rapidly rotating black holes, but there is a lack at medium and small a. These two simulations are in contradiction with observations (see Reynolds (2013) and references therein).

6 DISCUSSION

It is hard to satisfy boundary conditions in the framework of the Narayan & Yi (1995) self-similar ADAF model. Accretion disk structure is strongly deformed near the last stable orbit where gas pressure approaches zero. In our calculations we assumed magnetic pressure proportional to thermal pressure. But while gas pressure goes to zero near the ISCO, magnetic stresses vary smoothly and remain reasonably high due to magnetic flux conservation (see Abolmasov (2014)). Using the self-similar model is better justified in this case than using slim-disk models together with the assumption that magnetic fields are everywhere proportional to thermal pressure. A self-consistent MHD approach would be a better approximation.

While corrections to the electromagnetic term due to transonic nature of the disk are probably slight, angular momentum of the falling matter should be more sensitive to the processes at the inner boundary of the disk because the balance between the individual terms in the radial Euler equation shifts rapidly close to the sonic surface.

The matter falling inside the last stable orbit conserves its angular momentum while outside the sonic surface, angular momentum may be easily transferred by tangential viscous stresses. Hence the angular momentum of the in-falling matter should be estimated at the sonic surface rather than at the ISCO.

Continuity equation may be written approximately as:

$$\frac{d(r^d \rho v_r)}{dr} = 0, \tag{42}$$

where d describes the geometry of the streamlines: $d = 1$ corresponds to cylindrical radial flow, $d = 2$ in case of spherical radial flow.

Let us combine it with the radial component of the Euler equation:

$$v_r \frac{dv_r}{dr} - \frac{v_\phi^2}{r} = -\frac{1}{\rho}\frac{dp}{dr} - \frac{v_K^2}{r} \tag{43}$$

Using these equations one can obtain the radial Grad-Shafranov equation (Beskin 2010):

$$\frac{d\ln\rho}{d\ln r}=\frac{v_\phi^2-v_K^2+d\cdot v_r^2}{rc_s^2(1-\frac{v_r^2}{c_s^2})} \tag{44}$$

At the sonic surface, denominator becomes zero hence the numerator should be zero too. This yields us angular momentum in the form:

$$L=L_K\sqrt{1-\frac{dv_r^2r}{GM}}=L_K\sqrt{1-\frac{dc_s^2r}{GM}}=L_K\sqrt{1-d\cdot\left(\frac{H}{r}\right)^2}=c_1^*L_K \tag{45}$$

Here c_1^* is coefficient that describes the deviations from Keplerian angular law (see section 3.3). In the self-similar ADAF model, $(H/r)^2=2.5c_3$. In our calculations we used $c_3=0.285$. Using this value for cylindrical radial flow one can find $c_1^*=0.536$ that is close to the value $c_1=0.43$ that we used in our calculations. For spherical flow c_1^* is very close to unity. We may conclude that our calculations are close to reality if disk height is constant near the sonic surface.

This may be the case if the flow inside the last stable orbit becomes magnetically supported in vertical direction.

In Shafee et al. (2008), Abolmasov (2014) and other works, rotation of magnetized accretion disks was found to be close to Keplerian near the last stable orbit. However, these works aimed on reproducing relatively thin disks with $H/r\sim0.1$. In thicker disks, deviations from Keplerian law should be larger. Besides, magnetic field configuration in fact is expected to affect the rotation of the inner disk regions through magnetic pressure and tangential stress.

In general, recent simulations support the BZ scenario (McKinney et al. 2012) and practically exclude the DML scenario. There are two reasons for this. First, inside the last stable orbit, density becomes very small and thermal pressure can no more counteract the Maxwellian stresses that leads to deformation and expansion of the magnetic field lines toward infinity. The second reason is existence of a large magnetic field in Blandford-Znajek configuration (with geometry close to a split-monopole) that leaves very small area for accretion and for field lines connecting the stretched horizon with the accretion disc. Numerical results suggest that either DML contribution to black hole rotation is practically absent or at least operates only on a small fraction of the stretched horizon surface (see also above section 5.4).

However, the results of these simulations are in apparent contradiction with observational data on super-massive black holes in galactic nuclei. Observations show that only about $7\div8\%$ of active galactic nuclei launch radio-bright jets (Ivezić et al. 2002). The reason for prevalence of radio-quiet objects is yet unclear, it may be connected to the overall magnetic flux through the black hole vicinity or to the broken symmetry of the magnetic field geometry. A probable reason for the discrepancy between simulations and observations is that most of the recent numerical simulations consider accretion discs with large-scale poloidal magnetic fields capable for rapid accumulation of magnetic flux inside the last stable orbit. Perhaps, smaller-scale chaotic magnetic fields would produce field geometry that is closer to the DML case.

DML configuration plotted in Fig. 1 can not be realized because Lorentz force acting on the magnetic loops inside the free-fall region will collapse them vertically. A more realistic picture with both processes, BZ and DML, taking place, is plotted in Fig. 11. Magnetic fields are supposed to be chaotic in the accretion disc: even regular fields are converted to small-scale loops due to Hall effect and magnetic instabilities (such as the magneto-rotational instability applied for accretion discs by Balbus & Hawley (1991)). Hence, in the accretion flow, substantial part of the magnetic field energy will be stored in small-scale loops having zero magnetic flux through the equatorial plane of the black hole. This part of the magnetic field is also a subject to dissipation at the horizon. As long as these chaotic magnetic fields are confined inside the accretion flow they can contribute to the DML process. Note that any magnetic loop with non-zero radial extension contributes to DML through frame-dragging; in full general relativity, one does not need to approach the horizon. Whether this condition is normally fulfilled or not is non-trivial and requires further thorough analytical and numerical consideration.

In our paper we did not consider mergers that may however have an important effect upon the evolution of SMBH. For example, in the work of Volonteri et al. (2005) the authors have made population synthesis of black holes with mergers and obtained Kerr parameter distribution similar to our result: Kerr parameter distributed between 0.1 and 0.9 with a peak at $a=0.5-0.6$. Most probably, if we will perform population synthesis of a black hole population taking into consideration both mergers and electromagnetic processes, we would obtain a qualitatively similar but broader distribution. But the question remains open: why do we observe a lot of black holes with high Kerr parameter? And the most probable explanation is supercritical accretion.

For a sample of black holes accreting magnetized matter for a large enough amount of time, broad distribution in spin is expected. Some of the objects stall near the critical a value, some are expected to evolve toward $a\sim1$. However, spin and mass evolution timescales are mostly larger than the Eddington timescale, and often larger than Hubble time. Together with the importance of mergers for black holes in galactic nuclei, it makes unreasonable to expect black hole rotation to be consistent with any unique spin value. Modeling taking into account all the effects is required.

In general, any black hole that gains an amount of mass comparable to its initial mass approaches its equilibrium rotation.

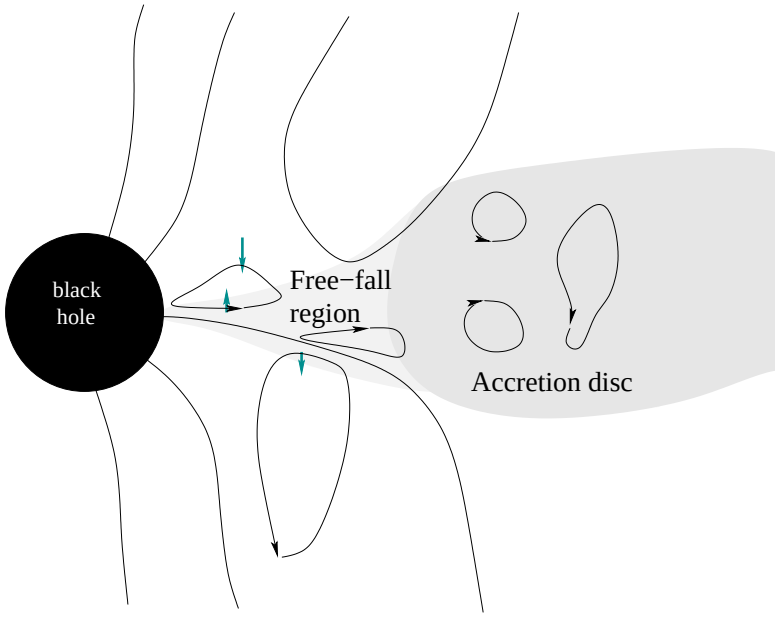

Figure 11. More realistic magnetic field configuration. Lorentz forces are shown as blue (grey) arrows.

Higher-mass black holes in binary systems should have also higher Kerr parameters, in consistence with the observed higher masses of the black holes in microquasars in comparison with the lighter black holes in X-ray novae (Banerjee & Mukhopadhyay 2013).

7 CONCLUSIONS

In our work we aimed on constraining the role of angular momentum exchange between the BH and accretion disc and that of general relativistic magnetic field decay that should affect this process. We find that DML-like processes may be important for thick advective discs, but magnetic field is damped significantly close to the horizon. Equilibrium Kerr parameter in this case is in the range $\sim 0.3 - 0.5$ and is primarily determined by deviations from Keplerian law in the disc. In supercritical regime, both electromagnetic processes do not influence black hole spin evolution significantly.

We have made Monte-Carlo simulations for a supermassive black hole population assuming that both processes operate simultaneously. For a reasonable parameter set, we obtain a broad distribution in Kerr parameter $0.1 \lesssim a \lesssim 0.9$ with a peak at $a \sim 0.7$ that is in fair agreement with observational data. For stellar mass black holes, the observed correlation between black hole masses and Kerr parameters may be understood as a consequence of accretion mass gain of $1 - 10 M_{\odot}$ in most of black hole binary systems.

Our results show that black hole observational appearance is sensitive to the accretion history, primarily to the period when most of the mass is gained. In the standard disc regime, a black hole gains a larger part of its mass and Kerr parameter increases faster than in ADAF regime.

ACKNOWLEDGMENTS

Anna thanks to RSF grant 14-12-00146 and Pasha also thanks to RFBR grant 14-02-91172 and Dynasty foundation. We would like to thank Professor Nikolai Shakura for inspiring of the basic idea of this work, and Professor Vasily S. Beskin and Sasha Tchekhovskoy for fruitful discussions on black hole magnetospheres. We are also grateful to the anonymous referees for valuable comments.

REFERENCES

Abolmasov P., 2014, ArXiv e-prints, 1408.6449
Abramowicz M. A., 2005, in Merloni A., Nayakshin S., Sunyaev R. A., eds, Growing Black Holes: Accretion in a Cosmological Context Super-Eddington black hole accretion: Polish doughnuts and slim disks. pp 257–273
Abramowicz M. A., Czerny B., Lasota J. P., Szuszkiewicz E., 1988, ApJ, 332, 646

Abramowicz M. A., Jaroszyński M., Kato S., Lasota J.-P., Różańska A., Sądowski A., 2010, A&A, 521, A15
Abramowicz M. A., Lasota J.-P., Igumenshchev I. V., 2000, MNRAS, 314, 775
Agol E., Krolik J. H., 2000, ApJ, 528, 161
Balbus S. A., Hawley J. F., 1991, ApJ, 376, 214
Banerjee I., Mukhopadhyay B., 2013, Physical Review Letters, 111, 061101
Bardeen J. M., 1970, Nature, 226, 64
Barkov M. V., Khangulyan D. V., 2012, MNRAS, 421, 1351
Beloborodov A. M., Abramowicz M. A., Novikov I. D., 1997, ApJ, 491, 267
Beskin V. S., 2010, MHD Flows in Compact Astrophysical Objects
Blandford R. D., 2002, in Gilfanov M., Sunyeav R., Churazov E., eds, Lighthouses of the Universe: The Most Luminous Celestial Objects and Their Use for Cosmology To the Lighthouse. p. 381
Blandford R. D., Begelman M. C., 1999, MNRAS, 303, L1
Blandford R. D., Znajek R. L., 1977, MNRAS, 179, 433
Casares J., Martín E. L., Charles P. A., Molaro P., Rebolo R., 1997, NewA, 1, 299
Chandrasekhar S., 1961, Hydrodynamic and hydromagnetic stability
Ferraro V. C. A., 1937, MNRAS, 97, 458
Fragile P. C., Wilson J., Rodriguez M., 2012, MNRAS, 424, 524
Fragos T., McClintock J. E., 2014, ArXiv e-prints,1408.6449
Fukue J., 2011, PASJ, 63, 803
Goldreich P., Reisenegger A., 1992, ApJ, 395, 250
Haiman Z., 2013, in Wiklind T., Mobasher B., Bromm V., eds, Astrophysics and Space Science Library Vol. 396 of Astrophysics and Space Science Library, The Formation of the First Massive Black Holes. p. 293
Harlaftis E. T., Greiner J., 2004, A&A, 414, L13
Hutchings J. B., Winter K., Cowley A. P., Schmidtke P. C., Crampton D., 2003, AJ, 126, 2368
Ivezić Ž.., Menou K., Knapp G. R. e. a., 2002, AJ, 124, 2364
Kato Y., Miyoshi M., Takahashi R., Negoro H., Matsumoto R., 2010, MNRAS, 403, L74
Krolik J. H., 1999, ApJL, 515, L73
Lipunova G. V., 1999, Astronomy Letters, 25, 508
Mahadevan R., 1998, Nature, 394, 651
McClintock J. E., Narayan R., Davis S. W., Gou L., Kulkarni A., Orosz J. A., Penna R. F., Remillard R. A., Steiner J. F., 2011, Classical and Quantum Gravity, 28, 114009
McClintock J. E., Narayan R., Gou L., Liu J., Penna R. F., Steiner J. F., 2010, X-ray Astronomy 2009; Present Status, Multi-Wavelength Approach and Future Perspectives, 1248, 101
McKinney J. C., Tchekhovskoy A., Blandford R. D., 2012, MNRAS, 423, 3083
Meyer F., Meyer-Hofmeister E., 1994, A&A, 288, 175
Moreno Méndez E., 2011, MNRAS, 413, 183
Narayan R., McClintock J. E., Tchekhovskoy A., 2013, ArXiv e-prints
Narayan R., Yi I., 1995, ApJ, 452, 710
Novikov I. D., Thorne K. S., 1973, in Black Holes (Les Astres Occlus) Astrophysics of black holes.. pp 343–450
Oda H., Machida M., Nakamura K. E., Matsumoto R., Narayan R., 2012, PASJ, 64, 15
Ohsuga K., Mineshige S., 2007, ApJ, 670, 1283
Ohsuga K., Mori M., Nakamoto T., Mineshige S., 2005, ApJ, 628, 368
Orosz J. A., Jain R. K., Bailyn C. D., McClintock J. E., Remillard R. A., 1998, ApJ, 499, 375
Orosz J. A., Steeghs D., McClintock J. E., Torres M. A. P., Bochkov I., Gou L., Narayan R., Blaschak M., Levine A. M., Remillard R. A., Bailyn C. D., Dwyer M. M., Buxton M., 2009, ApJ, 697, 573
Page D. N., Thorne K. S., 1974, ApJ, 191, 499
Penna R. F., McKinney J. C., Narayan R., Tchekhovskoy A., Shafee R., McClintock J. E., 2010, MNRAS, 408, 752
Penna R. F., Narayan R., Sądowski A., 2013, MNRAS
Penna R. F., Sądowski A., McKinney J. C., 2012, MNRAS, 420, 684
Podsiadlowski P., Rappaport S., Han Z., 2003, MNRAS, 341, 385
Poutanen J., Lipunova G., Fabrika S., Butkevich A. G., Abolmasov P., 2007, MNRAS, 377, 1187
Reynolds C. S., 2013, Classical and Quantum Gravity, 30, 244004
Sadowski A., Narayan R., Tchekhovskoy A., Abarca D., Zhu Y., McKinney J. C., 2014, ArXiv e-prints,1408.6449
Shafee R., McKinney J. C., Narayan R., Tchekhovskoy A., Gammie C. F., McClintock J. E., 2008, ApJL, 687, L25
Shahbaz T., 2003, MNRAS, 339, 1031
Shakura N. I., Sunyaev R. A., 1973, A&A, 24, 337
Shankar F., 2009, New Astronomy Reviews, 53, 57

Shankar F., Weinberg D. H., Miralda-Escudé J., 2013, MNRAS, 428, 421
Steeghs D., McClintock J. E., Parsons S. G., Reid M. J., Littlefair S., Dhillon V. S., 2013, ApJ, 768, 185
Suleimanov V. F., Lipunova G. V., Shakura N. I., 2008, A&A, 491, 267
Tchekhovskoy A., Narayan R., McKinney J. C., 2010, NewA, 15, 749
Thorne K. S., 1974, ApJ, 191, 507
Thorne K. S., Price R. H., MacDonald D. A., 1986, Black holes: The membrane paradigm
Uzdensky D. A., 2005, ApJ, 620, 889
Valsecchi F., Willems B., Fragos T., Kalogera V., 2010, in Leitherer C., Bennett P. D., Morris P. W., Van Loon J. T., eds, Hot and Cool: Bridging Gaps in Massive Star Evolution Vol. 425 of Astronomical Society of the Pacific Conference Series, The Eclipsing Black Hole X-ray Binary M33 X-7: Understanding the Current Properties. p. 227
Volonteri M., Madau P., Quataert E., Rees M. J., 2005, ApJ, 620, 69
Yang X.-H., Yuan F., Ohsuga K., Bu D.-F., 2014, ApJ, 780, 79
Ziółkowski J., 2011, MNRAS, 418, 2381